GEOFIZIKA VOL. 41 2024

DOI: https://doi.org/10.15233/gfz.2024.41.5
Original scientific paper

Croatian catalogue and database of focal mechanism solutions, characteristic mechanisms, and stress field properties in the Dinarides and the surrounding regions

Marijan Herak

Department of Geophysics, Faculty of Science, University of Zagreb

Received 16 October 2024, in final form 25 November 2024

This report presents the CroFMS catalogue and database of focal mechanism solutions (FMS). It is based on the first-motion polarity data for earthquakes in Croatia and the neighbouring regions, collected over last four decades. The current catalogue version contains FMS for 410 earthquakes that were computed consistently, using the same programs, velocity models, and sets of parameters. Its content is described in terms of distributions of the time and origin of polarity picks, magnitudes, epicentral distances of stations, the quality marks, the phases used, azimuthal gap and distance to the closest station. It was also shown that solutions from the CroFMS catalogue and those independently obtained from the moment tensor inversions are generally consistent.

Comparison of observed FMS with the latest European model of active fault sources (EFSM20) revealed several inconsistencies, most notably in the Zagreb and Petrinja epicentral areas, the greater Rijeka region, the Central Adriatic archipelago, and in the zone of surface traces of the thrust fronts of the East-Bosnian–Durmitor and Drina–Ivanjica nappes in Bosnia and Herzegovina.

Spatial averaging of FMS over the whole study area produced maps of characteristic focal mechanisms, which may be found useful in the seismic hazard assessment in the areas where active faults are not identified or characterised.

A formal stress inversion of the focal mechanism solutions produced a map of maximum horizontal stress orientations across the study area, revealing localized lateral variations that had not been identified in previous studies.

Keywords: earthquake focal mechanisms, characteristic focal mechanism, stress field, principal stress axes

Abbreviations

BDC – Best Double-Couple
CFM – Characteristic Focal Mechanism
CroFMS – Croatian FMS catalogue (and database)
EFSM20 – European Fault Source Model 2020 (Basili et al. 2022)
FMS – Focal Mechanism Solution
FMP – First Motion Polarity (of the P-wave)
FPS – Fault-Plane Solution
FSI – Formal Stress Inversion
MTI – Moment Tensor Inversion

1. Introduction

Earthquake focal mechanism solutions (FMS), also known as fault-plane solutions (FPS), offer insight into the geometry of earthquake sources, and thus provide invaluable data for the characterization of active faults and estimation of seismic hazard, tectonic stress field studies, and research in tectonics and structural geology. FMS are generally represented by three parameters defining the double-couple force system that best describes the forces acting in the earthquake source.

Historically, FMS were first computed using the spatial distribution of the observed P-wave first motion polarities (FMP) from a number of well azimuthally distributed stations. The first attempts and theoretical basses were presented by Japanese seismologists, most notably T. Shida in 1917 (see Nakano, 1923; Kawasumi, 1934; or Agnew, 2002) and H. Nakano (1923), whose results and ideas inspired P. Byerly (1928) to propose a method to infer the nature of forces acting in the earthquake source. More on early developments of the methods may be found in Stauder (1962). Later-on, when broad-band seismographs appeared in the 1980-ies and the computers matured enough to handle required computations, best double couple (BDT) solutions became available through moment tensor inversion techniques (MTI). Although MTI solutions tend to prevail today, especially for large events, FMP method still provides valuable information (see the section 3.2.2. below).

The first mechanisms published for Croatian earthquakes date back to 1960-ies and 1970-ies (*e.g.* Constantinescu et al., 1966; Ritsema, 1967; McKenzie, 1972). The first mechanism computed by Croatian seismologists was for the earthquake of 25 July 1979 in the Croatia–Bosnia and Herzegovina border region, close to Imotski (M_L = 4.2; Živčić et al., 1980). The first solution for a Croatian event computed in Croatia is, to the best of my knowledge, the one for the small earthquake of 5 May 1979 that occurred in the Bay of Kvarner, south of Rijeka (M_L = 3.6; Živčić and Allegretti, 1983). Mechanisms of Croatian events

were subsequently presented in a number of papers, especially in the series of reports on the seismicity of Croatia (Herak et al., 1991; Markušić et al., 1993, 1998; Ivančić et al., 2001, 2006, 2018) or the case studies of important events (*e.g.* Herak and Jukić, 1993; Herak et al., 2005, 2021; Herak and Herak, 2010, 2023; Govorčin et al., 2020; Dasović et al., 2024).

The first catalogue of focal mechanisms for 40 Croatian earthquakes was published by Herak et al. (1995). With time the collection of FMS grew, the data quality requirements got stricter, and polarity inversion methods were improved, so a comprehensive revision of the input dataset and the catalogue became necessary in order to ensure consistency in both the data and the solutions. The review itself included re-computation of all FMS using the same velocity models and the ray tracing algorithm, sets of weights, and solution quality assessment rules (see Appendix A). Whenever deemed necessary, the polarities stored in the event files where re-checked by consulting original seismograms or bulletin entries. The final outcome of the revision – the Croatian catalogue of focal mechanism solutions (CroFMS) – is presented here. It is thus the result of uniform processing of data collected over the period of more than 35 years. This also implies that some previously published solutions have changed, in some cases significantly. These changes primarily affect the solutions for older earthquakes based on bulletin data or scans of analogue seismograms, which include some of the largest events in the catalogue – *e.g.* the 1909 Kupa Valley earthquake (Herak and Herak, 2010), the Banja Luka earthquakes of 1969 (Ustaszewski et al., 2014), or the 1986 Knin earthquake (Herak and Jukić, 1993).

The CroFMS catalogue covers External and Internal Dinarides, and the parts of the Pannonian Basin and the Adriatic Sea (Adria), *i.e.* the areas whose seismicity may affect seismic hazard in Croatia (green long-dashed polygon in Fig. 1). This includes the territories of Croatia and Bosnia and Herzegovina, as well as the neighbouring regions of Slovenia, Hungary, Serbia and Montenegro. Fig. 1 also shows seismicity (after the Croatian Earthquake Catalogue, CEC, Herak et al.,1996, last updated in 2024). The most prominent active areas are the ones of Dalmatia (SE Croatia) together with SW Bosnia and Herzegovina, NW Croatia (especially around Zagreb, and along the border with Slovenia), the zone around Rijeka, the southern Adriatic, and the band of seismicity starting from the Petrinja epicentral area and continuing SE-wards towards Sarajevo. Recent seismicity has been described in a number of dedicated papers (see the references listed above).

This report describes the Croatian FMS database in some detail. It will also present two products directly derived from the CroFMS catalogue – the map of characteristic focal mechanisms, and the stress map of the investigated region. Some observations that the readers may find interesting or intriguing will also be pointed out. However, detailed discussion of implications or causes of the observed patterns are beyond the scope of this report.

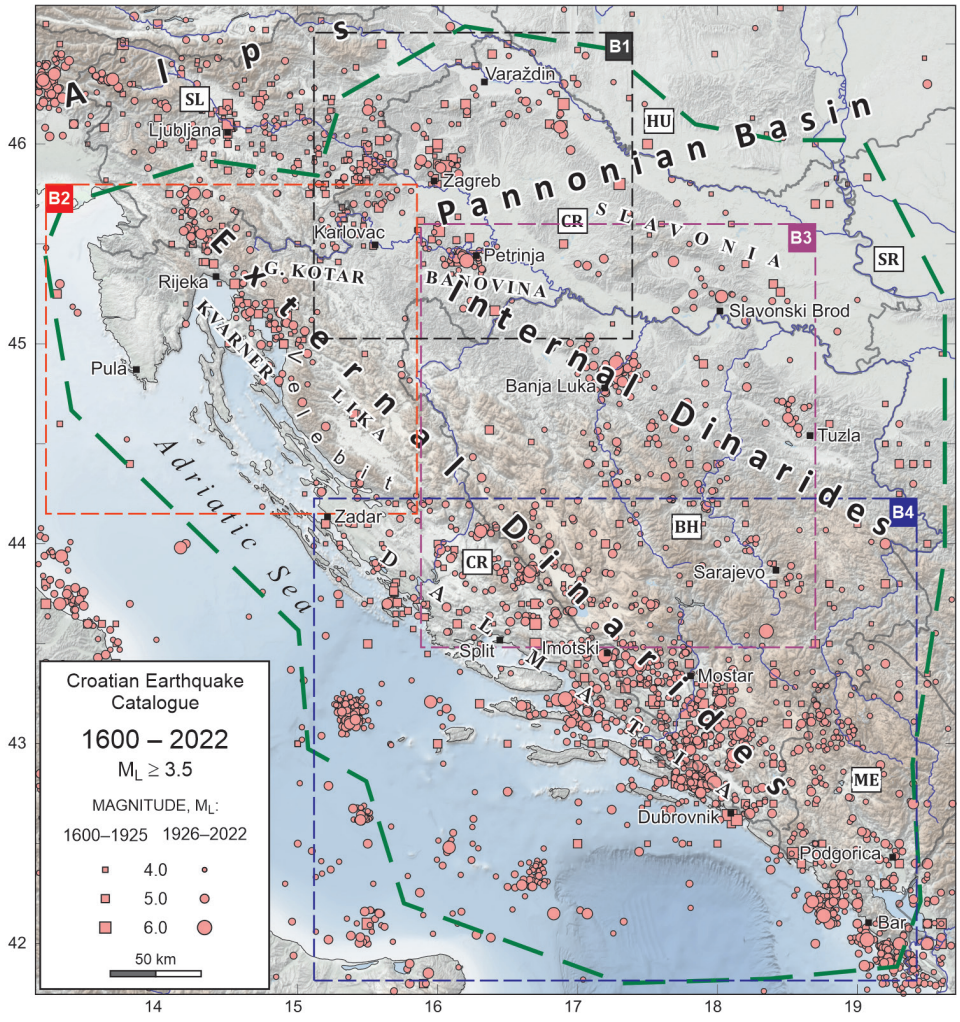

Figure 1. Domain of the CroFMS catalogue coverage (green long-dashed polygon). Superimposed are the epicentres of earthquakes (1600–2022) with the local magnitude $M_L \geq 3.5$ from the Croatian Earthquake Catalogue (Herak et al., 1996, last updated in 2024). The symbols (squares for the period 1600–1925, and circles thereafter) with magnitude (see the legend). State borders are full grey lines (BH – Bosnia and Herzegovina, CR – Croatia, HU – Hungary, ME – Montenegro, SL – Slovenia, SR – Serbia). The boxes B1–B4 mark the extent of Figs. 8, 10, 11 and 12, respectively.

2. The Croatian focal mechanism database (CroFMS)

The CroFMS database consists of:

– *A collection of analogue and digital seismograms (event files) for 486 earthquakes* (48 Gb of data). 170 scans of analogue historical seismograms for

6 events in the period 1909–1970 are from the Sismos database (INGV, 2024; see also Ferrari, 2016). Digital seismograms are the ones from the Croatian network (CR), as well as from many networks available from the EIDA on-line database. Particularly important were the networks 8X, 9H, GE, GR, HU, IV, MN, NI, OE, OX, RF, SJ, SL, Y5, Z3 (EIDA, 2024; see list of DOIs in References).

– *A set of 410 input files with polarities and other input parameters.* These files contain station codes, epicentral distances, azimuths, and polarities (either read from seismological bulletins, or hand-picked by an experienced seismologist), with indication of the sharpness of the onset of the first-arriving P-phase (eP_1 or iP_1). In some cases, an indication is given of the relative amplitude of the first swing (see Appendix A for detail).
– *Velocity model files* used to compute emergence angles of the first phase at the source (see Appendix A).
– *The CroFMS catalogue of focal mechanism solutions* (see the next section). The catalogue is available in digital form in the Electronic Supplement.

3. The Croatian catalogue of focal mechanism solutions (CroFMS)

3.1. Some statistical properties

The CroFMS catalogue covers the time span from 8 October 1909 (the Kupa Valley earthquake, Herak and Herak, 2010) to 30 June 2024. The territory coverage is bound by a green dashed polygon in Fig. 1. It contains 410 earthquakes, with 27112 read first-onset polarities: 3606 iP_1 and 1631 eP_1 taken from various bulletins (mostly the ones of the International Seismological Centre, 1992–2024), and 20094 iP_1 and 1781 eP_1 hand-picked from digital or analogue seismograms. The magnitudes range from $M_L = 2.0$ to $M_L = 6.8$ (Fig. 2a), and distance distribution (Fig. 2b) shows prevalence of Pn phases.

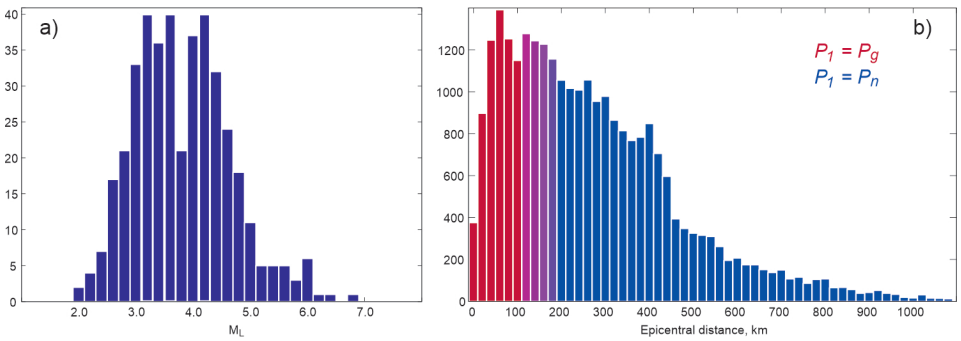

Figure 2. *a*) Histogram of local magnitudes in the dataset. *b*) Distribution of 27112 epicentral distances. Red and blue bars correspond to distances where the first arriving phase is Pg and Pn, respectively. Around Pg–Pn crossover distances between about 115 km and 170 km, the first arriving phase depends on the velocity model and the focal depth.

Histogram in Fig. 3 shows breakdown of the yearly number of FMS in the catalogue. Quite clearly, the numbers generally increase with time. The rapid increase starts at about the turn of the centuries, when digital data began to become available and the number of instruments quickly increased. Of course, the increase is not uniform, mostly due to aftershocks of strong events (*e.g.* in the years 2020 and 2021 when two large events occurred in Croatia). Likewise, the number of polarity readings increase in exponential manner (Fig. 3b), with current average around 2000 per year.

Figure 4 shows temporal evolution of percentage of the seismogram and bulletin data, both for iP_1 and eP_1. As expected, the data read from various bulletins fall below 10% in the last 15 years or so, and hand-picked seismogram first onsets clearly dominate the dataset. In inversions the weight of the bulletin data was as a rule two times smaller than the weight for the polarities directly read from the seismograms (Appendix A). The same holds for the weights of eP_1 vs iP_1.

The accuracy and reliability of the mechanism solutions heavily depend on several quantities, among which two stand out – the largest azimuthal gap (γ) of reporting stations, and the smallest epicentral distance (D_{min}) that indicate how well is the focal sphere sampled by the outcoming rays. They are shown in

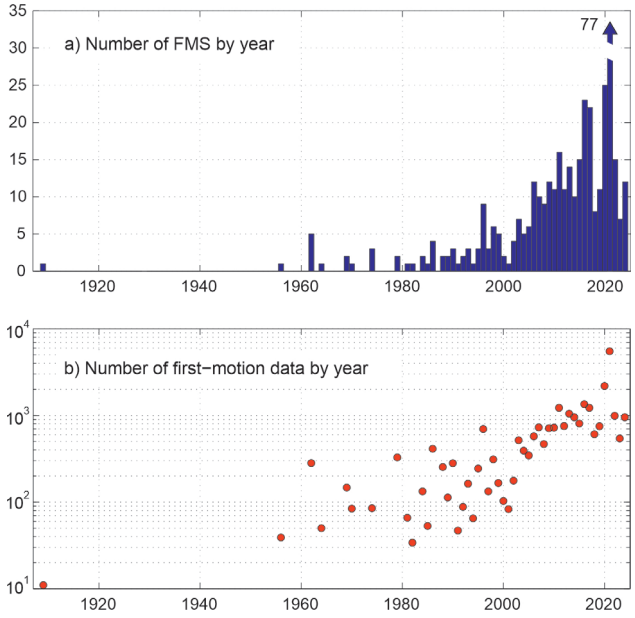

Figure 3. *a*) The number of focal mechanism solutions by year. Some aftershock sequences are marked by a large number of solutions (*e.g.* the Petrinja earthquake sequence of 2020–2021 with 77 FMS). *b*) The number of polarity data increases roughly exponentially with time.

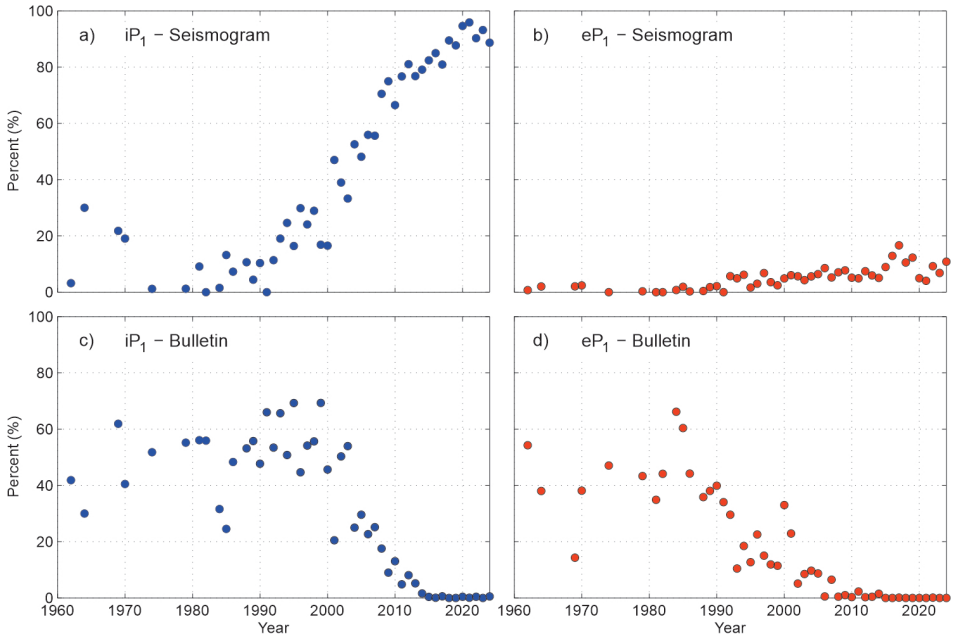

Figure 4. Yearly number of the first polarity readings from seismograms (*a*, *b*) and from various bulletins (*c*, *d*); Clear readings (iP_1: *a*, *c*) and emergent readings (eP_1: *b*, *d*).

Fig. 5, both as a temporal evolution, and as histograms. The gap $\lambda < 180°$ indicates that the epicentre is within the network of reporting stations, which is seen to be true for all events after 1960 but one. For the large majority of mechanisms $\lambda < 90°$ indicates that the azimuthal distribution of stations was good. Figure 5b shows the same for the minimal epicentral distance. Over 95% of mechanisms have at least one station closer than 100 km, and in about 80% of cases D_{min} is less than 50 km. It is also clear that in recent time both parameters settled at rather low values.

The quality (Q) of a solution is expressed numerically, from 1 (unacceptable) to 5 (excellent). It depends on the largest Kagan angle between the best solution and all other competing solutions at the 75% confidence level, and on the percentage of correct polarities (see Appendix A for definitions and more detail). Fig. 6a shows the distribution of quality of solutions – about 80% of mechanisms received quality mark of $Q \geq 3$, whereas 1/3 of them are classified with the highest grade ($Q = 5$). 2/3 of mechanisms were computed with at least 90% of correct polarities (Fig. 6b).

3.2. Focal mechanisms

All focal mechanisms from the CroFMS catalogue with quality $Q \geq 2$ are shown in Fig. 7. The colour of compressional quadrant indicates the style of

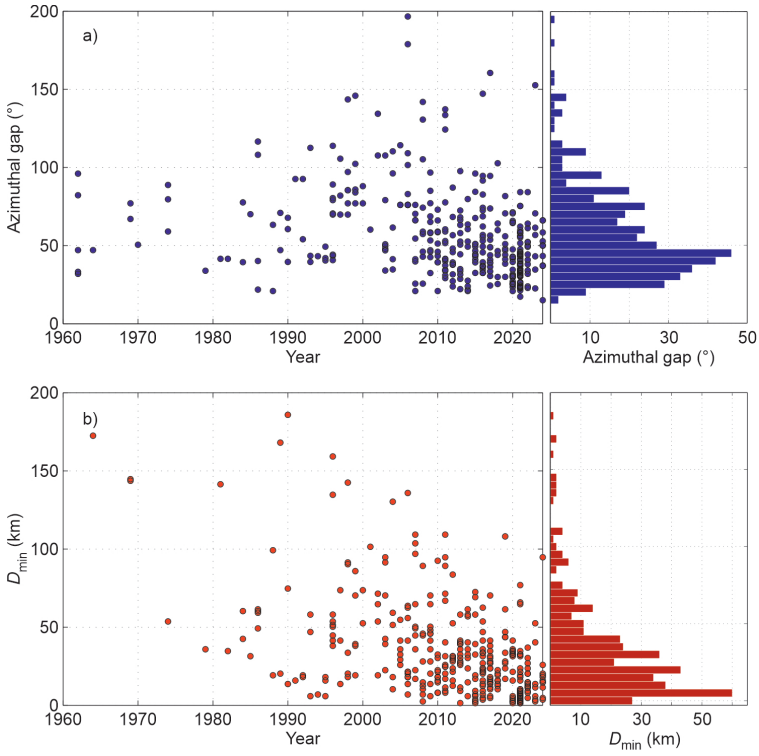

Figure 5. Temporal distribution of the largest azimuthal gap (*a*, *left*) and minimal epicentral distance (*b*, *left*). The corresponding histograms are on the right-hand side of the subplots *a*) and *b*).

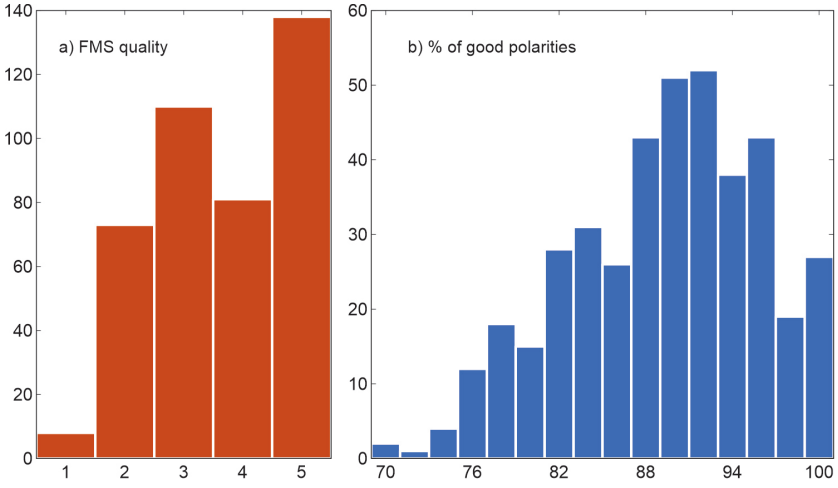

Figure 6. *a*) Histograms of the FMS quality; *b*) Distribution of the percentage of correct polarities.

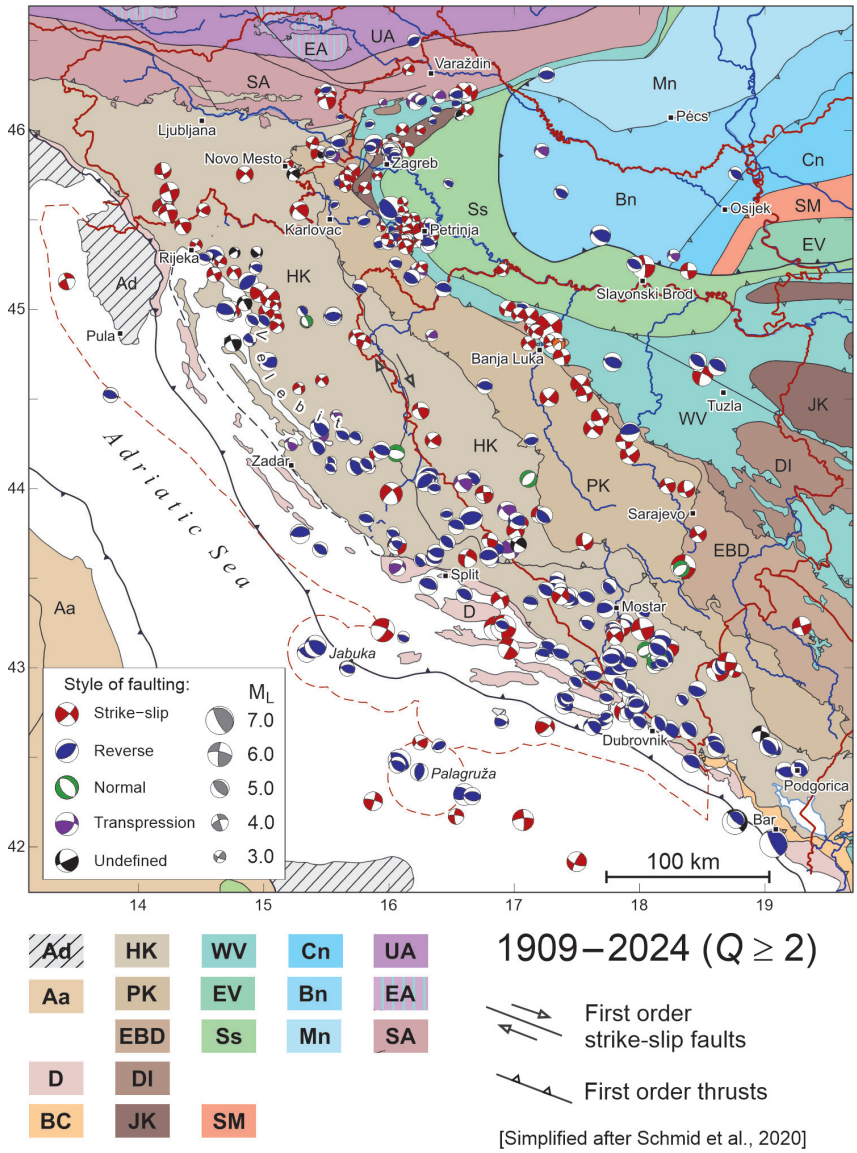

Figure 7. Focal mechanisms from the CroFMS catalogue, 1909–2024, with solution quality $Q \geq 2$. The beachballs are lower-hemisphere stereographic projection, their size scales with magnitude and compressive quadrants are coloured according to the style of faulting (see the legend). The basemap of tectonic units is simplified after Shmid et al. (2020). The units are (simplified names): **Ad** – Adriatic microplate, **Aa** – Adria-derived allochthons, **D** – Dalmatian unit, **BC** – Budva–Cukali, **HK** – High Karst, **PK** – Pre-Karst, **EBD** – East Bosnian–Durmitor nappe, **DI** – Drina–Ivanjica nappe, **JK** – Jadar–Kopaonik nappe, **WV** – Western Vardar ophioloitic, **EV** – Eastern Vardar ophioloitic, **Ss** – Sava suture, **SM** – Serbo-Macedonian, **Cn** – Codru nappe, **Bn** – Bihor nappe, **Mn** – Mecsek nappe, **UA** – Upper Austroalpine, **EA** – Eoalpine high pressure belt, **SA** – South Alpine.

faulting after Heidbach et al. (2016a). The beachballs are superimposed on the map of tectonic units published by Schmid et al. (2020).

The reverse/thrust mechanisms clearly predominate in the High Karst unit in Dalmatia and the neighbouring regions of Bosnia and Herzegovina, which is in line with current notion of seismicity there being generated along subparallel SE–NW striking reverse faults by northward movement and counter-clockwise rotation of Adria with respect to the Dinarides as a part of the Eurasian plate (*e.g.* Nocquet and Calais, 2004; Grenerczy et al., 2005; Weber et al., 2010).

On the other hand, strike-slip sources form a well-defined, about 200 km long, elongated zone along and close to the thrust front of the East Bosnian–Durmitor nappe, from NW of Banja Luka to Sarajevo. The consistent observation of purely strike-slip motion on sub-vertical fault planes close to traces of the mapped thrusts is intriguing, and may be a subject of a dedicated future study (see also section 3.2.1. below).

Strike-slip seems to be the prevalent mechanism also in the greater Rijeka region, from SW Slovenia to Velebit Mt in Croatia. However, the tectonics here seems to be more complex than in southern Dalmatia, as a number of reverse faults were also activated, even with strikes perpendicular to the usual Dinaric direction.

The most diverse area is the one of NW Croatia where main geological structures strike SW–NE to W–E. In a predominantly N–S directed stress field (see below) the faults may be activated as reverse, strike-slip, or reverse-oblique slip (transpression). The largest earthquake with an FMS there is pure reverse (Zagreb 2020 mainshock, $M_L = 5.5$).

Central Adriatic hosts mostly reverse events, related to the islets of Jabuka and Palagruža. The southern Adriatic's seismicity is very low, so we only have two reliable solutions, both strike-slip.

3.2.1. CroFMS and the European Fault Source Model EFSM2020

Focal mechanism solutions are important in the process of defining or verifying active sources to be used, for instance, in seismic hazard assessment (SHA). It is unfortunate that Croatia still has no database characterizing its active-faults on the whole territory, so by necessity, Europe-wide products may be used. Herewith we use the European Fault Source Model (EFSM20, Basili et al., 2022) that was incorporated into the latest European Seismic Hazard Model ESHM20 (Danciu et al., 2024) to check its compatibility with the CroFMS catalogue.

Figures 8 and 10–12 present the mainshock solutions within the four boxes shown in Fig. 1. Next to each beachball is the solution reference number as listed in the catalogue digital file available in the Electronic Supplement. Each figure also displays the seismogenic sources from the European Fault Source Model (EFSM20, Basili et al., 2022). The CroFMS catalogue was declustered to remove aftershocks possibly triggered on secondary faults by Coulomb stress

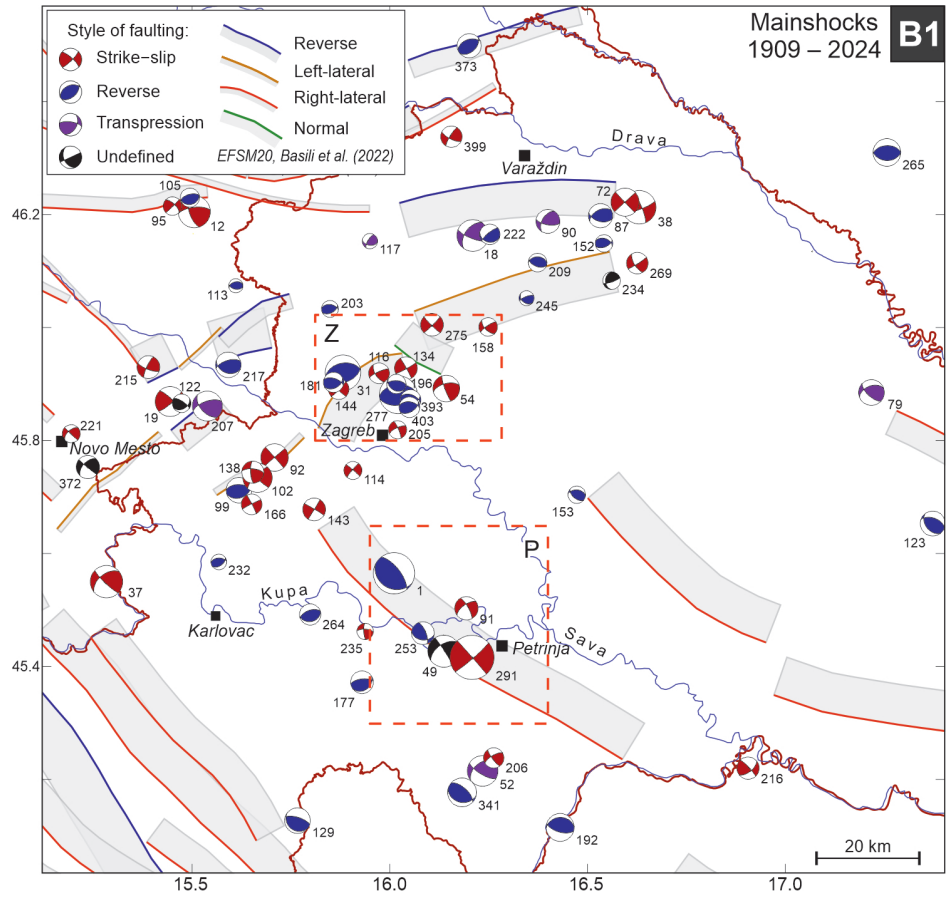

Figure 8. Mainshock solutions in the box B1 of Fig. 1. Numbers next to the beachballs are the reference numbers from the CroFMS catalogue. Traces of fault sources are from the EFSM20 model (Basili et al., 2022), grey polygons are their projections to the surface. Detailed exploded plots of all events (foreshocks, mainshocks, and aftershocks) within the red dashed rectangles Z (Zagreb) and P (Petrinja), are shown in Fig. 9.

changes induced by the mainshock, as they are not representative of the characteristic source properties in the broader epicentral area (see an example of the Petrinja 2021 sequence, Herak and Herak, 2023; also Fig. 9P).

Box B1 shows the area of NW Croatia (Fig. 8). In its northernmost part, close to the capital Zagreb and Varaždin, and the Croatia–Slovenia border area SW from Zagreb, active faults strike mostly SW–NE to W–E, *i.e.* perpendicularly to the Dinaric strike. The two EFSM20 sources south of Varaždin are classified as reverse and left-lateral. The FMS of the three largest earthquakes there are reverse-oblique or strike slip. However, they refer to events from before the digital era, and so should be considered *cum grano salis*. The left lateral EFSM20

source to the SW from Zagreb is confirmed as such by FMS. In the Zagreb epicentral area (rectangle Z, Fig. 9Z), EFSM20 lists two major sources. The first one coincides with the North Medvednica Boundary Fault (NMBF, Tomljenović and Csontos, 2001; see also Herak et al., 2021) and is marked in EFSM20 as left-lateral strike-slip fault. The northeastern-most segment of this fault (striking about WSW–ENE) was the source of the recent 2020 Zagreb earthquake (M_L = 5.3). The FMP solution, along with the moment tensor inversion and aftershock locations, indicated that the faulting was a pure reverse one on a plane dipping towards the SSE (Herak et al., 2021). This is at odds with the source character in the EFSM20 model. Considering the local stress field (Fig. B3, Appendix B, as well as results from this study, see section 5 below), which is there directed N–S, this important fault would probably be better characterized as oblique-reverse with considerable left-lateral component in the fault's southwestern and central segments, and as pure reverse fault further to the northeast. The second fault in the EFSM20 data set in this area is described as NW–SE striking and NE dipping fault with a normal sense of slip. The trace of this fault aligns well with the Kašina Fault, which is considered a right-lateral strike-slip fault. (KF, *e.g.* Tomljenović and Csontos, 2001; Matoš et al., 2014; van Gelder et al., 2015). There are no normal earthquakes in the CroFMS catalogue in this area, but there are two strike-slip events not far from KF to the SW (numbers 54 and 134 in Fig. 9Z). It might thus be more likely (and in agreement with the local stresses) that the KF is presently active as the right lateral fault, possibly with an oblique, top–southeast directed component of slip (*e.g.* see in van Gelder et al., 2015). However, a caution is necessary as reliable evidence confirming or describing recent activity of this fault is very scarce.

In the areas south of Karlovac, in the Kupa Valley, and north of Sava in the Pannonian plain, seismic sources have a Dinaric strike (SE–NW). Most of the EFSM20 sources there have not had a significant recent activity except for the Kupa Valley (Petrinja) source which hosted two very important earthquakes – the famous 1909 Kupa Valley earthquake (M_S = 5.8) (Mohorovičić, 1910a,b,c; Herak and Herak, 2010), and the 2020 Petrinja earthquake (M_w = 6.4) (*e.g.* Herak and Herak, 2023). Fig. 9P shows all FMS within the rectangle P (Fig. 8) in the greater Kupa Valley epicentral area. The bulk of solutions are aftershocks of the 2020–2021 sequence, in which about an equal number of events occurred on strike-slip faults as on the reverse ones. The foreshock, the mainshock, and the largest aftershock, however, exhibited pure right-lateral slip on a sub-vertical Petrinja fault (PF in Fig. 9P) that was activated in the length of about 20 km (Herak and Herak, 2023). The corresponding large source in EFSM20 is classified as right-lateral strike slip, with expected dip between 55° and 70°, and rake between 120° and 170°, so significant reverse motion is considered possible. The observed dip and rake for the 2020 Petrinja earthquake are 89° and 175° respectively. Let us also note that the strikes of the PF and the activated segment of the EFSM20 source differ by about 10° on average. The 1909 earthquake (the

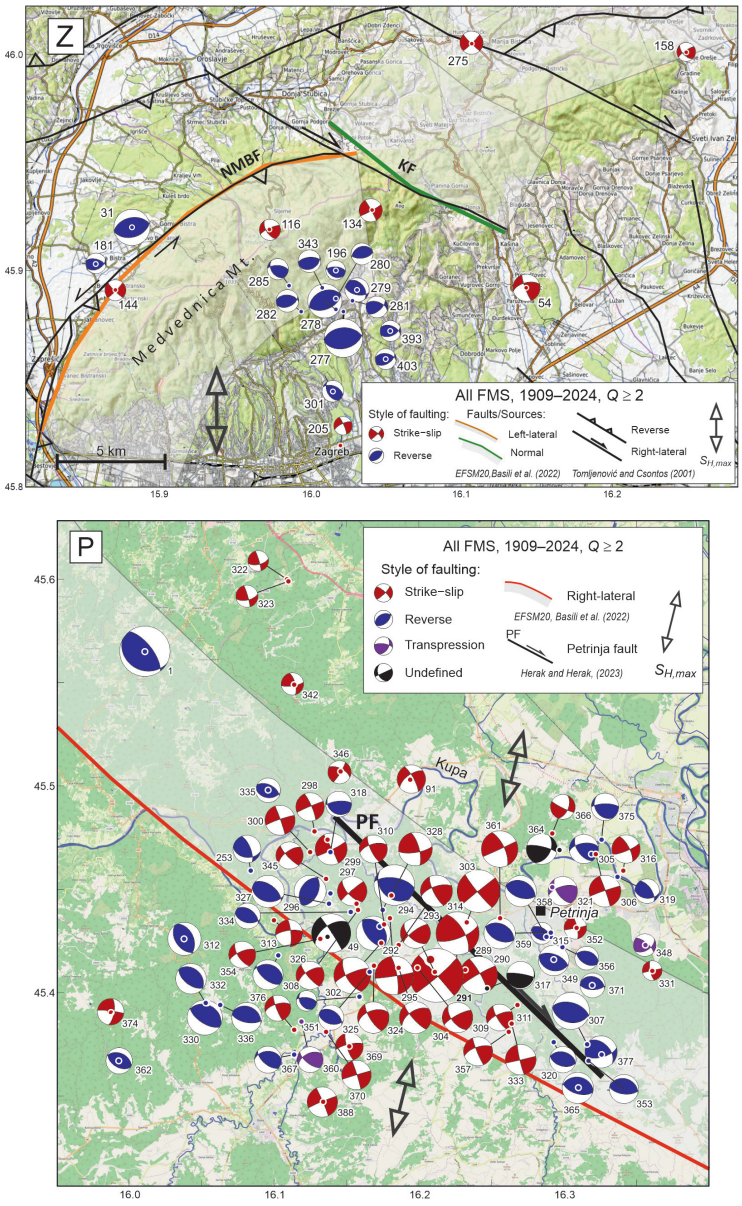

Figure 9. All solutions in the Zagreb (Z) and Petrinja (P) rectangles. Each beachball is connected with its epicentre (circle in the colour of the compressional quadrant). Numbers next to the beachballs are the chronological reference numbers from the CroFMS catalogue. Coloured traces of fault sources are from the EFSM20 model (Basili et al., 2022), transparent light-grey polygons are their projections to the surface. NMBF – North Medvednica Boundary Fault, KF – Kašina fault (Tomljenović and Csontos, 2001), PF – Petrinja fault (Herak and Herak, 2023). Double arrows are aligned in the direction of the maximum horizontal stress S_{Hmax} (see below).

first FMS in the catalogue, with a low quality mark!), which occurred north of the Kupa river, fits the EFSM20 source description with its dip and strike, but the reverse component is somewhat larger than proposed.

Figure 10 shows mainshock FMS in the area bounded by the box B2 (see Fig. 1 for location). Covered are the Croatia–Slovenia border region (to the NW from Klana), the Kvarner area (from Rijeka to Novi Vinodolski, and the islands of northern Adriatic), Istria, Velebit Mt., and Lika. The major faults strike in the general Dinaric direction (SE–NW). The FMS are exclusively strike-slip in SW Slovenia, and in the section from Klana to Rijeka. Further to the SE there is a melange of rather consistently oriented strike-slip solutions (compatible with dextral displacement on one of the proposed dominantly reverse fault sources from the EFMS20 database) and variable orientation reverse solutions of mostly small events. The largest proposed fault – the reverse fault closely following the shape of Velebit Mt. – has no clearly associated events, except on its southernmost segments after its trace enters the mainland. A discussion of proposed

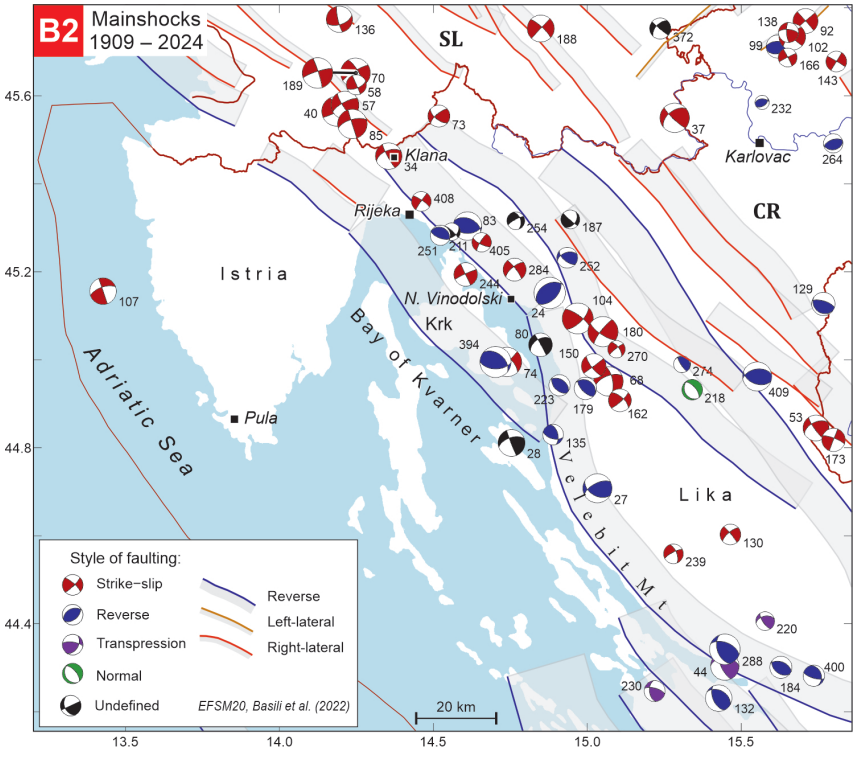

Figure 10. Mainshock solutions in the box B2 of Fig. 1. Numbers next to the beachballs are the chronological reference numbers from the CroFMS catalogue. Traces of fault sources are from the EFSM20 model (Basili et al., 2022), grey polygons are their projections to the surface.

fault patterns in this complex region where dominantly reverse mechanisms in Central External Dinarides of Dalmatia (Fig. 12) turn into exclusively strike-slip ones in the Northern Dinarides of SW Slovenia is well beyond the scope of this paper (but see, *e.g.* Moulin et al., 2014, 2016; Palenik et al., 2019, or Balling et al., 2023).

The most prominent feature seen in the box B3 (Fig. 11; see Fig. 1 for position) is the aforementioned rather narrow band of strike-slip earthquakes in Bosnia and Herzegovina It starts north of Kozara Mt (NW of Banja Luka) and continues towards Sarajevo in a length of about 200 km. One could tentatively extend this to the NW to include the Petrinja epicentral area in Croatia, and to the SE into Montenegro (Fig. 7), which would extend it to about 350 km. These earthquakes with strike-slip mechanisms are located near the surface traces of the thrust fronts of the East-Bosnian–Durmitor and Drina–Ivanjica nappes. As only two small events there were found with reverse faulting mechanisms, these frontal thrusts are probably no longer active. Peak activity of these frontal thrusts occurred during early Late Cretaceous and Paleogene (see Fig. 6 in Schmid et al., 2008), presumably under stress conditions significantly different from those prevailing today. The cross-section *a*–*b* shown in Fig. 11 suggests that the bulk of seismic activity occurs at depths above 20 km, and mostly within the Pre-Karst nappe. Recognizing that the strike of active faults in EFSM20 is of Dinaric orientation, the stress is predominantly released in dextral strike-slip motion on sub-vertical faults, which are optimally oriented to the present-day tectonic stress field (see section 5 below). However, the left-lateral faulting is anticipated on faults striking SW–NE that were not considered in EFSM20 (for instance, the Banja Luka fault proposed by Ustaszewski et al., 2014).

The EFSM20 source striking SE-wards from Banja Luka is classified as right-lateral and is in very good correspondence with the FMS nearby. The other three EFSM20 sources near Kozara Mt., Zenica and Sarajevo are prevalently reverse with a dextral strike-slip component and dipping between 50° and 80°. They do not adequately describe the FMS nearest to them.

Strong seismicity is also observed in southwestern Bosnia and Herzegovina, close to the border with Croatia. Those mechanisms will be described below in the context of box B4.

Figure 12 shows mainshock FMS in the box B4 (see Fig. 1 for location) that contains sources in Central and Southern Dalmatia and Adriatic, as well as in Montenegro and Bosnia and Herzegovina close to the border with Croatia.

As a rule, seismic sources are oriented SE–NW, parallel to the mountain ranges. The exception is found in central Dalmatia, especially around Split and in the Central Adriatic archipelago (the islands of Brač, Hvar, Korčula), where delineated sources strike W–E to WNW–ESE, parallel to the elongation of the islands. Overall, the large majority of focal mechanisms indicate reverse style of faulting, with occasional strike-slip or even normal solutions.

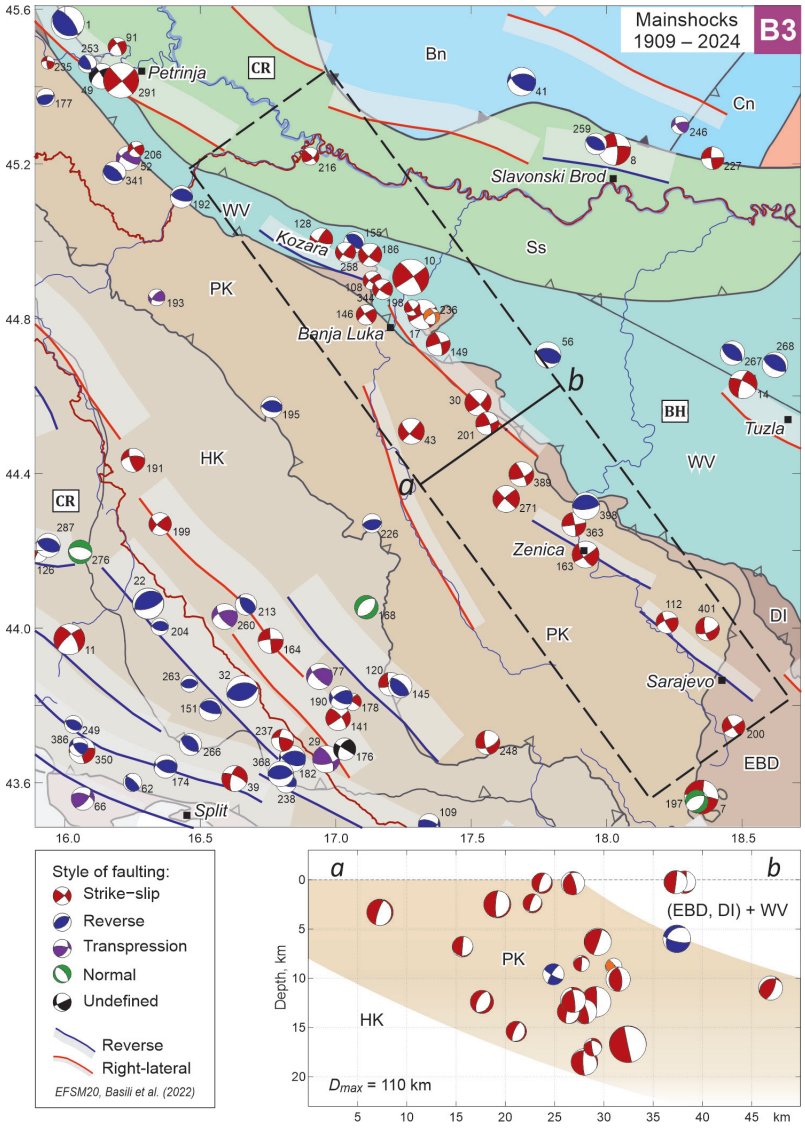

Figure 11. Mainshock solutions in the box B3 of Fig. 1. Numbers next to the beachballs are the chronological reference numbers from the CroFMS catalogue. The basemap of tectonic units is simplified after Schmid et al. (2020) (see the caption to Fig. 7 for more detail). Tectonic units shown here: **HK** – High Karst, **PK** – Pre-Karst, **EBD** – East Bosnian–Durmitor nappe, **DI** – Drina–Ivanjica nappe, **WV** – Western Vardar ophioloitic unit, **Ss** – Sava suture, **Cn** – Codru Nappe, **Bn** – Bihor nappe. BH – Bosnia and Herzegovina, CR – Croatia. The cross-section *a*—*b* is shown below the map. **(EBD, DI) + WV** – composite EBD and DI nappes overlain with WV ophiolites. The swath (D_{max} = 100 km) from which hypocentres are projected is bounded by the dashed rectangle in the map. The beachballs (the away hemisphere) are shown in horizontal view from the SE. The tectonic units in the profile are only sketched provisionally.

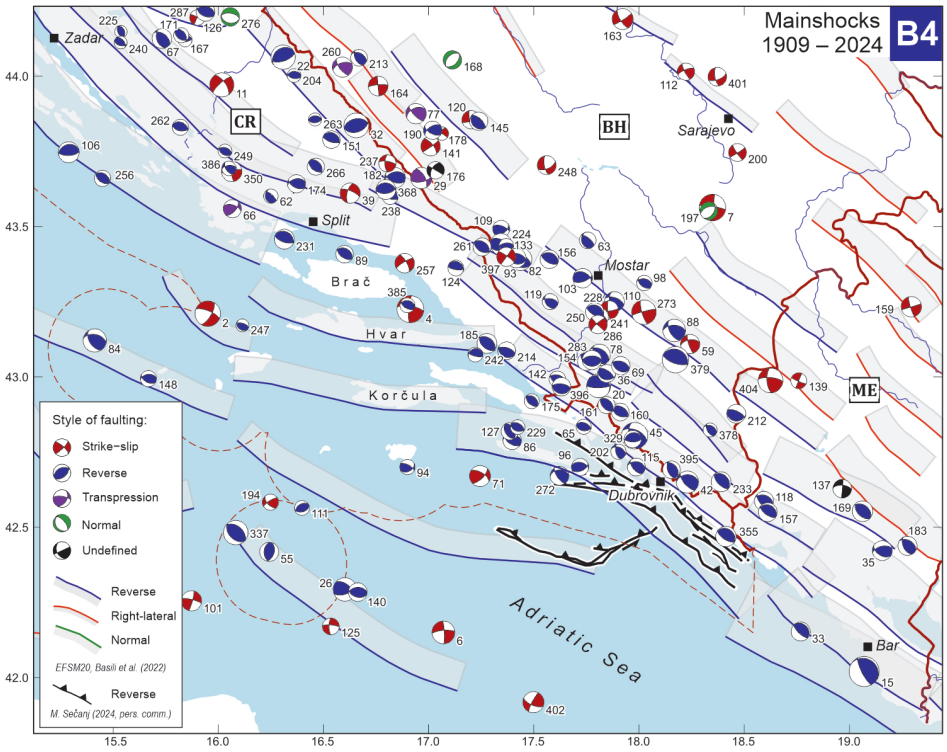

Figure 12. Mainshock solutions in the box B4 (see Fig. 1 for location). Numbers next to the beachballs are the chronological reference numbers from the CroFMS catalogue.

In Southern Dalmatia (approximately south of Korčula) and in southern Montenegro the FMS correspond well to the EFSM20 sources, both in strike and the sense of faulting. The preferred fault-planes are the ones dipping to the NE. Also shown are mostly reverse faults in the Adriatic Sea in the Dubrovnik area found to be active in the Pliocene and Quaternary (black lines in Fig. 12; simplified after M. Sečanj, pers. comm., 2024; see also Faivre et al., 2024). Somewhat more inland, southeast of Mostar (Bosnia and Herzegovina), there is a mixture of reverse and strike-slip solutions grouped along a reverse EFSM20 fault source.

Only a few FMSs exist in the Central Adriatic archipelago. They include the 1962 Makarska earthquake mainshock with the epicentre in the channel between Brač and Hvar. The focal mechanisms of the foreshock ($M_L = 5.9$), the mainshock ($M_L = 6.1$), and the largest aftershock show strike-slip faulting (Fig. 7), with one nodal line suggesting left lateral slip on a fault corresponding to the predominantly reverse EFSM20 source running along the Hvar island. Here again, a caution is advised in interpreting FMS of earthquakes that occurred 62 years ago. However, assuming that the stress field here does not change dramatically compared to the areas more to the SE, and is thus oriented generally in the NE–SW

direction (see Figs. B3 and 15–17 below), it would be expected that faults striking W–E are more likely to support strike-slip than reverse faulting.

A group of solutions with considerable strike-slip components is found to the north of Split, in Bosnia and Herzegovina, just over the border with Croatia. They may be related to the corresponding EFSM20 right-lateral source. Likewise, most focal mechanisms between Zadar and Split are in reasonable agreement with the proposed network of active sources.

3.2.2. Comparison of the first motion polarity (FMP) solutions with the best double-couples from the moment tensor inversion (MTI BDC)

As already noted in the Introduction, although nowadays MTI solutions tend to prevail, FMP approach still provides valuable information. Firstly, because the two methods may result in significantly different solutions as they are related to different aspects of the source process. While FMP reveals mostly high-frequency properties at the rupture initiation time and location, the MTI is associated to long period radiation from fault segments releasing the bulk of energy, and those two locations may be far apart. FMP solutions incosistent with the full MTI can also be a consequence of the multi-type rupture (Turhan et al., 2023). And secondly, the MTI is today restricted mostly to earthquakes of magnitudes larger than $M \approx 3.6–5.5$ (depending on the agency and algorithm, see *e.g.* Saraò et al., 2021), so smaller ones are commonly analysed by FMP algorithms. This is especially important in low-seismicity areas, as well as during aftershock sequences from which a large number of FMP solutions may provide insight into the complex fault patterns and stress redistribution following the mainshock (*e.g.* Herak and Herak, 2023, as an example from Croatia).

It is therefore of interest to compare the FMP solutions contained in the CroFMS catalogue with the corresponding available representative MTI best double-couple results as reported by various international agencies.

I have been able to identify 127 earthquakes from the CroFMS catalogue for which at least one MTI BDC solution is available. If multiple MTI solutions existed, a representative one was computed as the solution that minimizes the mean Kagan angle α (see Appendix A for definition) between itself and all available MTI solutions. The pairs FMP–MTI BDC are shown in Fig. 13, and Fig. 14 presents distribution of the Kagan angles.

A visual inspection of Fig. 13 shows that in most cases the two algorithms yielded similar results. This is confirmed in Fig. 14b as in 60% of cases α is below 30°, and 80% of mechanisms are characterized by $\alpha < 45°$. However, in some cases, the two solutions are quite different (*e.g.* 21-12-2008, 28-04-2011, 14-12-2011, 13-03-2014, or 19-06-2014). This does not mean that either of the results is wrong – it may just reflect faulting properties at different locations along the ruptured fault plane. However, as many of those 'mismatched' earthquakes are relatively small and thus not expected to be caused by large ruptures, such observations may prompt re-examination of both solutions.

Figure 13. Comparison of the first-motion polarity solutions from the CroFMS catalogue (left, black compressive quadrants, size scales with the solution quality, 2–5) and the corresponding moment-tensor inversion (MTI) best double-couples (right, red compressive quadrants) reported by various agencies. Above each pair is the date, time, moment magnitude M_W, the MTI source, and the Kagan angle α in degrees. MIX indicates the average of several available MTI solutions (see text in section 3.2.2). GFZ: Geoforschungszentrum (Germany), GCM: Global Centroid Moment Tensor Project (GCMT, Dziewonski et al. 1981; Ekström et al. 2012), ING: Istituto Nazionale di Geofisica e Volcanologia (INGV, Italy), ISC: International Seismological Centre (UK), NEI: National Earthquake Information Center (NEIC, USA), OCA: Observatoire de la Côte d'Azure. *Continues on the next page.*

Figure 13. *Continued from previous page.*

4. Characteristic focal mechanisms (CFM)

Knowing the prevailing style of faulting in an areal source defined for seismic hazard assessment, or a characteristic focal mechanism (CFM) at any location where an earthquake relevant for seismic hazard may occur, is today a prereq-

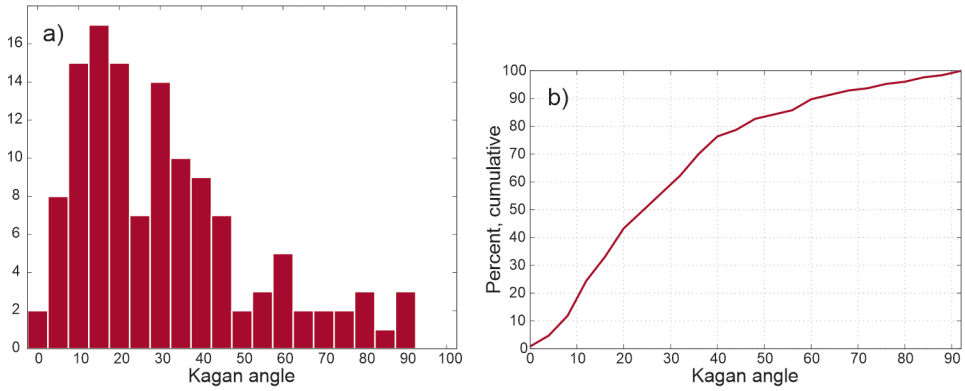

Figure 14. *a*) Histogram of Kagan angles between the first-motion polarity (FMP) and moment tensor inversion (MTI) solutions. *b*) Cumulative distribution of Kagan angles.

uisite for using modern ground motion prediction models. Such data may also be used to compute Joyner-Boore or rupture distance if actual active fault network is yet undefined. For example, Roselli et al. (2018) used the database of FMS to compile maps of CFM for Italy.

Herewith, CFM at any location is defined by averaging all available FMS within a predefined spatial circular window. Let N_{FMS} be the number of focal mechanisms (FMS_i, $i = 1, ..., N_{FMS}$) within the circular window with the radius R, and let the corresponding weights (w_i) be defined by:

$$w_i = (w_y\, w_m\, w_q)^{1/2},$$

where

$w_y = 1$ if $year \leq 2000$
$w_y = 2$ if $year > 2000$ and $year \leq 2015$
$w_y = 4$ if $year > 2015$

$w_m = 1$ if $M < 4.0$
$w_m = 2$ if $M \geq 4.0$ and $M < 5.0$
$w_m = 4$ if $M \geq 5.0$

$w_q = Q - 1, \quad Q \in [1, 2, 3, 4, 5].$

Here *year* is the year of the earthquake, M is its magnitude (either M_L or M_W), and Q is the quality mark of the FMS. In this way large weights are given to FMS related to more recent, larger magnitude and better constrained events.

The averaging is then done in a similar way as explained in the previous section, *i.e.* by finding such a mechanism that minimises the weighted average of Kagan angles (α_{try}) between the N_{FMS} focal mechanisms FMS_i and the trial mechanism (FMS_{try}):

$$\alpha_{try} = \frac{\sum_{i=1}^{N_{FMS}} w_i \alpha\left(FMS_i, FMS_{try}\right)}{\sum_{i=1}^{N_{FMS}} w_i}.$$

The FMS_{try} corresponding to the $\min(\alpha_{try}) = \alpha_{try,min}$ is then adopted as CFM. The quality of the characteristic focal mechanism, Q_{CFM}, is defined by:

$$Q_{CFM} = 1: N_{FMS} = 1 \text{ or } \alpha_{try,min} > 45°$$
$$Q_{CFM} = 2: N_{FMS} \geq 2 \text{ and } \alpha_{try,min} \leq 45°$$
$$Q_{CFM} = 3: N_{FMS} \geq 4 \text{ and } \alpha_{try,min} \leq 35°$$
$$Q_{CFM} = 4: N_{FMS} \geq 6 \text{ and } \alpha_{try,min} \leq 25°$$
$$Q_{CFM} = 5: N_{FMS} \geq 8 \text{ and } \alpha_{try,min} \leq 20°.$$

The strictest fullfiled conditions apply.

Figure 15 shows the map of characteristic mechanisms obtained by finding the double-couple mechanism that best describes average properties of faulting computed on a regular grid with nodes 16.7 km (0.150°) apart. Only CFM obtained using at least three observed first-motion polarity FMS within $R = 20$ km from each node are shown. Aftershocks were excluded from analyses.

The NW Croatia (polygon A) shows a mixture of solutions. Strike-slip faults prevail in Slovenia (left-lateral ones, in agreement with the database of active faults in Slovenia, Atanackov et al., 2021) and towards the Petrinja region in the south-east where dextral motions are expected. Reverse sources are mostly found around Medvednica Mt. and the Zagreb region (with the actual fault planes dipping towards SE), as well as in Banovina in the southern part of this area. The transpressive solutions occur mostly in the north. Polygon B, with foci mostly in the Pre-Karst unit (PK) shows exclusively strike-slip CFM, with the actual fault most probably of the right-lateral character. For more discussion see section 3.2.1. above. Polygon C marks a group of CFM in the High Karst (HK) tectonic unit, in the northern External Dinarides, *i.e.* in SW Slovenia, and across the border in the greater Rijeka region. Clearly prevailing are strike-slip events, most probably with the dextral nodal plane representing the active fault (*e.g.* Atanackov et al., 2021). In the south and southwest seismogenic faults seem to be dominantly reverse. Finally, polygon D contains CFM in the High Karst (HK) and Dalmatian (D) units of the central and southern External Dinarides (Dalmatia and the bordering area with Bosnia and Herzegovina). CFM here are reverse with only a few exceptions – most notably in the Central Adriatic archipelago in the Dalmatian tectonic unit (D), near the islands of Brač and Hvar where strike-slip events are expected, and in the NE part of the polygon D, in southwestern Bosnia and Herzegovina close to the border with Croatia, with strike-slip sources and reverse oblique faulting.

The resolution of the maps as shown in Fig. 15, is determined by the maximum allowed distance (R) from each node. Reducing R increases resolution, but it also lowers the number of events captured, potentially reducing coverage. This occurs because a smaller R makes it less likely that the minimum required

number of events will be present within each node's neighborhood. The choice of $R = 20$ km was made to balance the bias between the resolution and coverage.

Better resolution may be obtained by enlarging the input database, thus increasing the probability of collecting enough mechanisms around each node. For instance, in addition to the FMP solutions, one could also consider all available best double-couple moment tensor inversion results (see section 3.2.2., and Fig. B4 in Appendix B). Doing so, and reducing the maximal distance from the grid nodes to $R = 15$ km (the contributing area decreased by 44%), with somewhat denser grid (15 km × 15 km) resulted in the map of CFM as presented in Fig. B5 (Appendix B). The coverage was somewhat reduced, but the overall picture is the same as in Fig. 15 with some local differences in Slavonia and in the Central Adriatic.

The files containing characteristic focal mechanisms from Figs. 15 and B5 are available in the Electronic Supplement.

5. Stress-field inferred from the focal mechanism solutions

Assessing the stress field properties in a region is essential for understanding tectonic processes and earthquake sources. This information is highly valuable across various seismological disciplines. For example, it is needed in studying Coulomb stress changes after a large earthquake. It also plays a key role in understanding the mechanics of existing faults most prone to failure, which is necessary for developing seismicity models for seismic hazard assessment.

Among the various stress indicators used to compile the World Stress Map (WSM, Heidbach et al., 2016b), parameters derived from earthquake focal mechanisms account for as much as 74% of data (Heidbach et al., 2018). Within this category 96% are of a single focal mechanism type, which is always assigned quality not better than C (on a scale A to E). The remaining 4% is provided by formal stress inversion of focal mechanisms, which is ranked as quality A or B (Barth et al., 2008).

The territory considered here is rather poorly covered with stress indicators – in the WSM they are all of quality C, derived from single focal mechanisms. Their density is the highest in southern and central Dalmatia, central Adriatic and in Montenegro, and considerably lower in the greater Rijeka region, around Zagreb, and in central Bosnia and Herzegovina. Large areas of northern Croatia, Slavonia, Lika, Banovina, Gorski kotar, surroundings of Zadar, NW Bosnia and Herzegovina (see Fig. 1 for locations) are practically not covered at all. It thus seems worthwile to try to improve the density of stress indicators by formal stress inversion of available data on focal mechanisms in this region.

Formal stress inversion (FSI) techniques are used to produce regional or local models of stress field from a collection of single FMS. Herewith, I used the MSATSI, a Matlab program package by Martínez-Garzón et al. (2014) that is based on the SATSI (Spatial And Temporal Stress Inversion) algorithm by Hardebeck

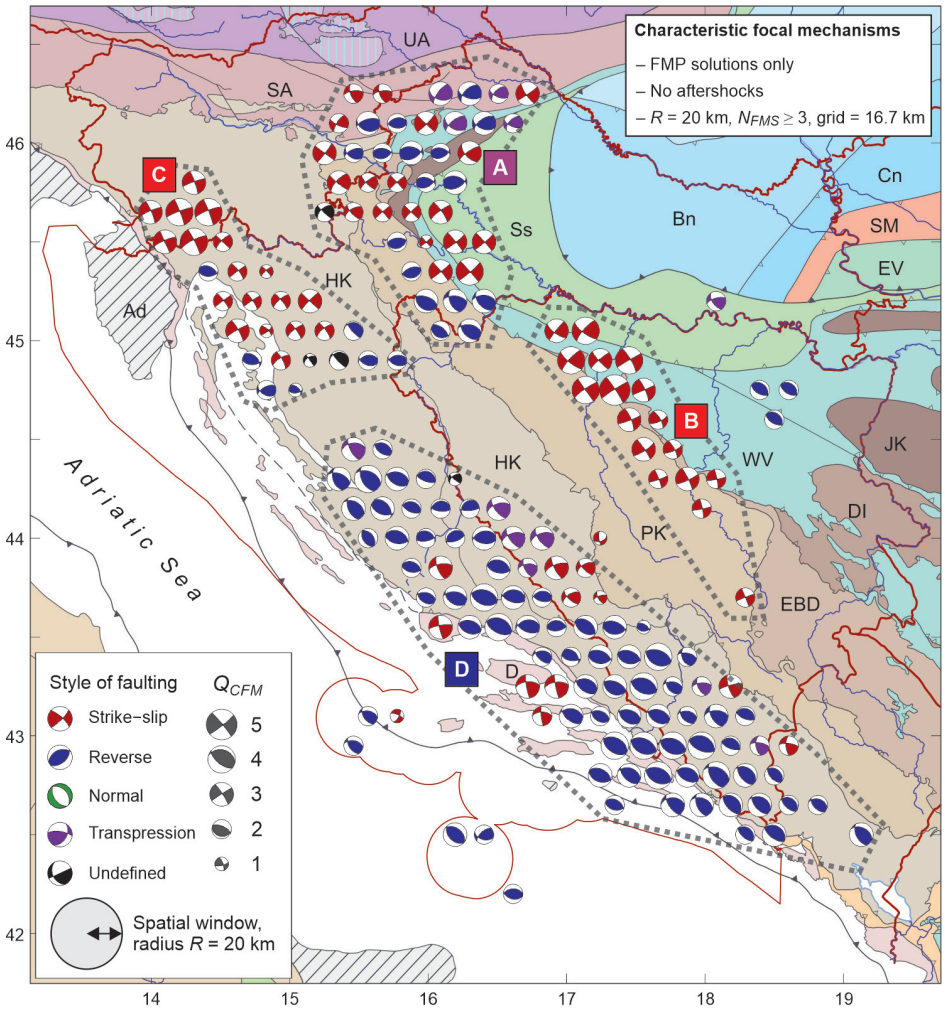

Figure 15. Characteristic focal mechanisms (CFM) computed by weighted averaging of the FMP focal mechanisms on a grid 16.7 km × 16.7 km, within the spatial window with radius of $R = 20$ km. Aftershocks were not considered. Only solutions based on at least three events in the window are shown. The size of the beachballs scales with the quality Q_{CFM}. The basemap of tectonic units is simplified after Schmid et al. (2020, see caption of Fig. 7 for detailed explanation).

and Michael (2006), which uses routine for calculation of horizontal stresses developed by Lund and Townend (2007). It provides a linearized damped least-squares inversion of the FMS data, along with relevant uncertainties. The chosen damping coefficient controls the trade-off between data misfit and model complexity. It thus effectively spatially smooths the stress-field inverted over a network of individual nodes, hopefully removing stress variation artefacts while

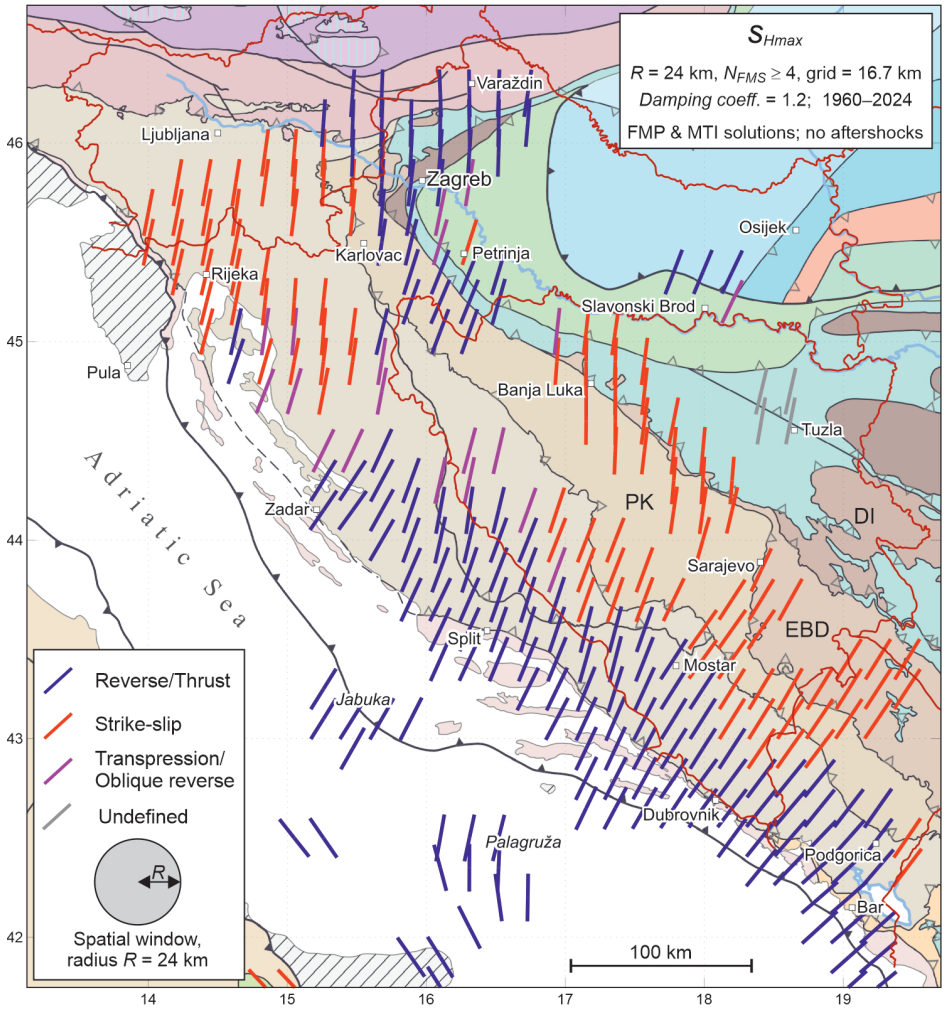

Figure 16. Maximal horizontal stress (S_{Hmax}) orientation obtained by formal stress inversion using FMP solutions from the CroFMS catalogue and available MTI solutions (1960–2024), without aftershocks. The nodes of the network are 16.7 km apart. Only nodes with at least four focal mechanisms within $R = 24$ km were considered. Tectonic regime is indicated by colours as shown in the legend.

retaining the spatial stress variations required by the FMS data (Hardebeck and Michael, 2006). The uncertainties of resulting deviatoric stress tensor components are modelled in MSATSI by bootstrap resampling (with replacements) of data at each grid point (Martínez-Garzón et al., 2016).

MSATSI procedure was applied to the dataset including both FMP and MTI data (Fig. 18 and Fig. B4 in Appendix B). Only events with the quality grade $Q \geq 2$ from the period 1960–2024 were used in inversion. Aftershocks were not used

to avoid events possibly strongly affected by local stress-field disturbances (see Martínez-Garzón et al., 2016). The spatial grid has nodes every 16.7 km (0.15° of latitude). Only nodes with at least four focal mechanisms within $R = 24$ km were considered. The damping coefficient equal to 1.2 was determined automatically by the program. The results are shown in Figs. 16, 17 and B6 (Appendix B).

Figure 16 shows a map of inverted directions of the maximum horizontal stress, S_{Hmax}, as well as the inferred distribution of stress regime (reverse, strike-slip or oblique reverse). Stress direction varies between SW–NE and S–N (except in parts of Central Adriatic where SE–NW directions are found). Along the coast the orientation of S_{Hmax} agrees well with the trajectories of the assumed Adria rotation around the Euler pole in the Western Alps (Weber et al., 2010; see also Nocquet and Calais, 2004). In the Dinarides, the largest gradient is suggested in the Pre-Karst (PK) unit between Sarajevo and Banja Luka where S_{Hmax} changes from direction perpendicular to the chain of the Dinarides to S–N in the Internal Dinarides. Another location of marked change in the S_{Hmax} orientation is in Central–Southern Adriatic near the islets of Jabuka and Palagruža. There the direction changes from SE–NW close to Italian shores, to the SW–NE orientation. The number of events considered in each node (N_{FMS}), as well as confidence intervals shown in Fig. 17, qualify many of the nodes for the WSM quality classes A (12°, $N_{FMS} \geq 15$) or B (20°, $N_{FMS} \geq 8$). The largest uncertainties were obtained near Knin and southeast of Split, along the southern coastal part of Montenegro, and near Tuzla in Bosnia and Herzegovina. The cause is a small number of observations combined with diverse FMS in these areas.

Spatial distributions of faulting regimes inferred from characteristic mechanisms (CFM) (Figs. 15 and B5) and from FSI (Fig. 16) compare very well. Some details observed in the CFM map in Fig. 15 (*e.g.* a small strike-slip area in the Central Adriatic archipelago) are smoothed out by rather large damping applied in formal inversion.

One of the outputs of the FSI as performed here is the map of relative stress magnitudes (also known as the stress ratios, and commonly referred to as R-values), defined in terms of the stress principal axes as:

$$R\text{-value} = (\sigma_1 - \sigma_2) / (\sigma_1 - \sigma_3),$$

with σ_1, σ_2, σ_3 being the major, intermediate and minor principal stress, respectively. It is a measure of relative magnitude of σ_2 compared to σ_1 and σ_3. Its spatial distribution is shown in Fig. B6 in Appendix B. Although some interesting trends may be seen, a detailed analyses is well beyond the scope of this report.

The primary source of uncertainty is the limited number of events considered at each network node. To improve this, let us divide the region into four distinct areas, labelled A–D as shown in Fig. 18, and invert the four subsets of FMS for the orientation of principal stress axes. Each area is characterized by unique seismicity properties and prevailing fault mechanisms (FMS). The areas A (NW

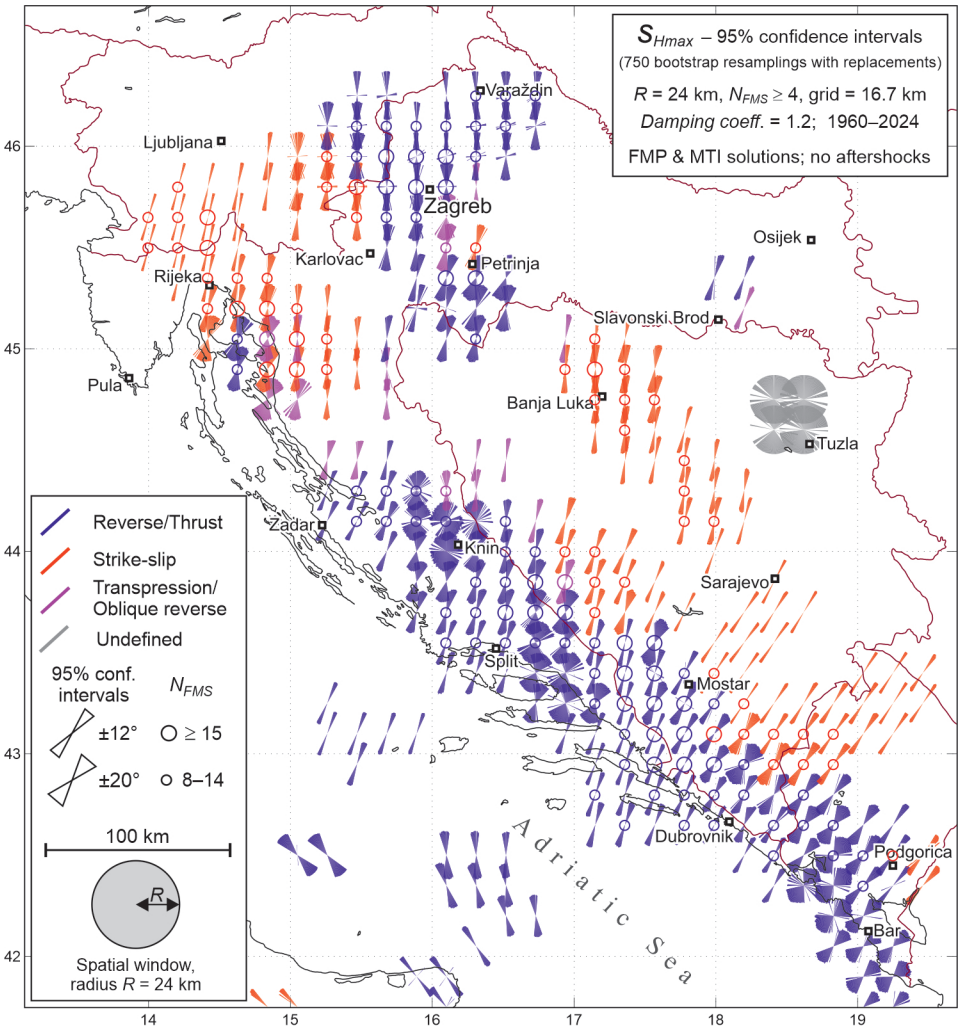

Figure 17. 95% confidence limits of direction of S_{Hmax} computed by 750 bootstrap resamplings with replacements (see Fig. 16 and its caption). Circles in each node denote the number of FMS in each node (N_{FMS}, see the legend).

Croatia) and B (NW–SE Bosnia and Herzegovina) host intraplate events, whereas the earthquakes in the areas C (from SE Slovenia to Velebit Mt.) and D (Dalmatia, SE Bosnia and Herzegovina and parts of Central Adriatic) are mostly directly related to the Adria–Dinarides collision. At the bottom of the figure, stereonets of the principal stress axes are presented for each of these areas.

The most important seismogenic sources in A are the ones related to the Mts. Medvednica (N of Zagreb), and Ivanšćica and Kalnik (south of Varaždin). This

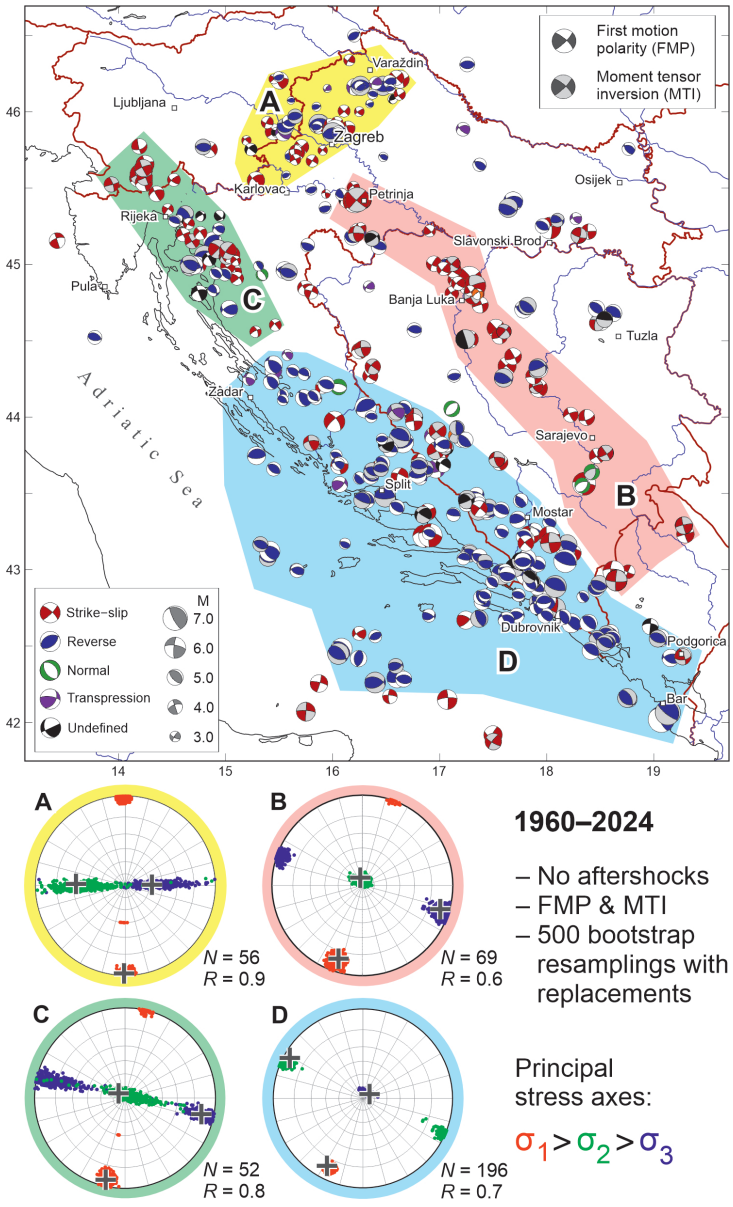

Figure 18. Principal stress axes in four regions (A–D, *top*). The white and shaded dilatational quadrants denote FMP and MTI solutions, respectively. *Bottom*: Stereonets of principal stress axes in each of the regions A–D. The number (*N*) of fault mechanisms (both FMP and MTI BDC) considered in inversion is shown at the bottom and to the right of each stereogram, together with the mean *R*-value from 500 bootstrap resamplings. Red – σ_1, green – σ_2, blue – σ_3. Mean solutions are shown by '+' signs in the corresponding clouds of points. Computed with MSATSI software (Martínez-Garzón et al., 2014).

is the most diverse area of the four, with faults of various strikes and sense of slip. The FMS of the largest events are all reverse, but there are many strike-slip and transpressive solutions too (see Figs. 8 and 9, along with the related discussion in section 3.2.1.). The stereonet (A in Fig. 18) computed from 56 focal mechanisms shows S–N orientation of perfectly horizontal major principal stress σ_1. The intermediate and minor stresses σ_2 and σ_3 are directed towards W and E, respectively, with mean σ_3 plunging at a higher angle. All of this suggests that characteristic faulting mechanism is oblique reverse with larger vertical component of slip.

Area B, stretching from Petrinja SE-wards to Banja Luka, Sarajevo and Montenegro (see also Fig. 11 and related discussion in section 3.2.1.), hosts mostly strike-slip earthquakes, which is clearly reflected in its stereonet (B in Fig. 18 based on 69 FMS). σ_1 is almost horizontal and trends at an azimuth of about 200° (SSW), and σ_2 is nearly perfectly vertical.

The stereonet for the greater Rijeka region (C in Fig. 18, based on 52 focal mechanisms), with horizontal σ_1 (striking at about 195°), and vertical σ_2 indicates that strike-slip is the most common style of faulting there. However, the smeared σ_3 suggests presence of a small reverse component. The largest area (D in Fig. 18) contains 196 FMS used for inversion. The characteristic faulting regime is pure dip-slip, with vertical σ_3 and horizontal σ_1 striking SW-to-SSW.

6. Conclusions

The CroFMS catalogue and the corresponding collection of seismograms and picked polarities systematise most of the work on focal mechanisms in Croatia done in the last four decades. As of 30 June 2024, it contains data on FMS for 410 earthquakes that occurred in Croatia and the neighbouring regions that can host earthquakes relevant for seismic hazard on Croatian territory. All FMS were computed consistently, using the same programs, sets of velocity models and weights, as well as the rules for the quality assignment. While not directly comparable, solutions based on first-motion polarities from the CroFMS catalogue and those derived from moment tensor inversion were found to be, on average, very similar.

Comparison of observed FMS with the latest European model of active fault sources (EFSM20, Basili et al., 2022) revealed several inconsistencies. Most notable such cases were found in the Zagreb and Petrinja epicentral areas, the greater Rijeka region, the Central Adriatic archipelago, and especially close to the surface traces of the thrust fronts of the East-Bosnian–Durmitor and Drina–Ivanjica nappes in Bosnia and Herzegovina.

Spatial averaging of FMS over the whole study area produced two catalogues and corresponding maps of characteristic focal mechanisms, which may be found useful in the seismic hazard assessment in the areas where active faults are not identified or characterised. This should be done *cum grano salis*, especially in places where the most important earthquakes contributing FMS occurred before the digital era.

Relatively large number of consistently computed FMS enabled formal stress inversion to be performed producing a map of S_{Hmax} in the investigated area. Several studies have been published on the stress direction in parts of this region (*e.g.* Bada et al., 2007; Carafa and Barba, 2013; Békési et al., 2023; Porkoláb et al., 2024). However, due to the limited density of data points, these studies necessarily relied on interpolation methods thus potentially missing local scale variations of the stress direction. An example is an intriguing observation of a large counterclockwise change of S_{Hmax} orientation by approximately 35° between the Pre-Karst (PK) frontal thrust and the Drina–Ivanica (DI) and East-Bosnian–Durmitor (EBD) frontal thrust zone (*e.g.* close to Sarajevo, Fig. 16), which perhaps deserves a dedicated study.

Data availability – The CroFMS catalogue, as well as the two catalogues of characteristic focal mechanisms are freely available in the Electronic Supplement.

Acknowledgments – Sometime in late autumn of 1980, Davorka Mišković (now Herak) – who was my supervisor at the time – asked me if I would care to join her in learning about the topic in seismology we heard nothing about in our studies – the focal mechanism solutions. I replied 'yes'... and here I am, 44 years later still computing focal mechanisms. Without her initiative, continuous support over the years and all those polarities read from the analogue seismograms, early digital seismograms, and seismological bulletins, the CroFMS catalogue would never have been compiled. Thank you!

This kind of effort heavily relies on the quality of seismic network operators, primarily in Croatia, but also in the neighbouring countries. Therefore, my thanks go to all the colleagues from the Geophysical Institute and the Croatian Seismological Survey (Department of Geophysics, Faculty of Science, University of Zagreb) and the network operators from Slovenia, Italy, Austria, Hungary... and all others who publicly shared their data.

I also thank Bruno Tomljenović for the most helpful discussions and help regarding tectonic and structural relationships in the area, as well as Jiři Zahradnik and an anonymous reviewer for their kind and helpful reviews.

References

Agnew, D. C. (2002): History of Seismology, In: *International Handbook of Earthquake and Engineering Seismology*, **81A**, Part A (Eds. Lee, W. H. K., Kanamori, H., Jennings, P. C. and Kisslinger, K.), Academic Press, 3–11.

Atanackov, J., Jamšek Rupnik, P., Jež, J., Celarc, B., Novak, M., Milanič, B., Markelj, A., Bavec, M., and Kastelic, V. (2021): Database of Active Faults in Slovenia: Compiling a New Active Fault Database at the Junction Between the Alps, the Dinarides and the Pannonian Basin Tectonic Domains, *Front. Earth Sci.*, **9**, 604388. https://doi.org/10.3389/feart.2021.604388.

Bada, G., Horváth, F., Dövényi, P., Szafián, P., Windhoffer, G., and Cloetingh. S. (2007): Present-day stress field and tectonic inversion in the Pannonian basin, *Glob. Planet. Change*, **58***,* 165–180, https://doi.org/10.1016/j.gloplacha.2007.01.007.

Balling, P., Tomljenović, B., Herak, M., and Ustaszewski, K. (2023): Impact of mechanical stratigraphy on deformation style and distribution of seismicity in the central External Dinarides: A 2D forward kinematic modelling study, *Swiss J. Geosci.*, **116**, 7, 30, https://doi.org/10.1186/s00015-023-00437-0.

Barth, A., Reinecker, J., and Heidbach, O. (2008): Stress derivation from earthquake focal mechanisms, *World Stress Map Project, Guidelines: Focal mechanisms*, 1–12.

Basili, R., Danciu, L., Beauval, C., Sesetyan, K., Vilanova, S., Adamia, S., Arroucau, P., Atanackov, J., Baize, S., Canora, C., Caputo, R., Carafa, M., Cushing, M., Custódio, S., Demircioglu Tumsa, M., Duarte, J., Ganas, A., García-Mayordomo, J., Gómez de la Peña, L., Gràcia, E., Jamšek Rupnik, P., Jomard, H., Kastelic, V., Maesano, F., Martín-Banda, R., Martínez-Loriente, S., Neres, M., Perea, H., Sket-Motnikar, B., Tiberti, M., Tsereteli, N., Tsironi, V., Vallone, R., Vanneste, K., Zupančič, P. (2022): European Fault-Source Model 2020 (EFSM20): online data on fault geometry and activity parameters. Istituto Nazionale di Geofisica e Vulcanologia (INGV), https://doi.org/10.13127/efsm20.

Békési, E., Porkoláb, K., Wesztergom, V., Wéber, Z. (2023): Updated stress dataset of the Circum-Pannonian region: Implications for regional tectonics and geo-energy applications, *Tectonophysics*, **856**, 229860, https://doi.org/10.1016/j.tecto.2023.229860.

Bianco, F., Del Pezzo, E., Castellano, M., Ibanez J., and Di Luccio, F. (2002): Separation of intrinsic and scattering seismic attenuation in the Southern Apennine zone, Italy, *Geophys J. Int.*, **150**, 10–22, https://doi.org/10.1046/j.1365-246X.2002.01696.x.

Byerly, P. (1928). Nature of first motion in the Chilean earthquake of November 11, 1922, *Am. J. Sci.*, **26**, 232–236.

Carafa, M. M. C. and Barba, S. (2013): The stress field in Europe: optimal orientations with confidence limits, *Geophys. J. Int.*, **193**, 531–548, https://doi.org/10.1093/gji/ggt024

Constantinescu, L., Ruprechtova, L., and Enescu, D. (1966): Mediterranean-Alpine Earthquake Mechanisms and their Seismotectonic Implications, *Geophys. J. Roy. Astron. Soc.*, **10**, 347368, https://doi.org/10.1111/j.1365-246X.1966.tb03063.x.

Crotwell, H. P., Owens, T. J., and Ritsema, J. (1999): The TauP Toolkit: Flexible seismic travel-time and ray-path utilities, *Seismol. Res. Lett.*, **70**, 154–160, https://doi.org/10.1785/gssrl.70.2.154.

Danciu, L., Giardini, D., Weatherill, G., Basili, R., Nandan, S., Rovida, A., Beauval, C., Bard, P.-Y., Pagani, M., Reyes, C. G., Sesetyan, K., Vilanova, S., Cotton, F., and Wiemer, S. (2024): The 2020 European Seismic Hazard Model: Overview and Results, *EGUsphere* [preprint], https://doi.org/10.5194/egusphere-2023-3062.

Dasović, I., Herak, M., Herak, D., Latečki, H., Sečanj, M., Tomljenović, B., Cvijić-Amulić, S., and Stipčević, J. (2024): The Berkovići (BIH) ML = 6.0 earthquake sequence of 22 April 2022 – Seismological and seismotectonic analyses, *Tectonophysics*, **875**, 230253. https://doi.org/10.1016/j.tecto.2024.230253.

Dziewonski, A. M., Chou, T.-A. and Woodhouse, J. H. (1981): Determination of earthquake source parameters from waveform data for studies of global and regional seismicity, *J. Geophys. Res.*, **86**, 2825–2852, https://doi.org/10.1029/JB086iB04p02825.

EIDA (2024): European Integrated Data Archive, http://eida.gfz-potsdam.de/webdc3/ (last accessed 7 September 2024). DOI of networks providing data:
8X –10.12686/ALPARRAY/8X_2016; **9H** – No registered DOI; **CR** –10.7914/SN/CR;
GE –10.14470/TR560404; **GR** –10.25928/mbx6-hr74;
HU –10.14470/UH028726; **IV** –10.13127/SD/X0FXnH7QfY;
MN –10.13127/SD/fBBBtDtd6q; **NI** –10.7914/SN/NI; **OE** –10.7914/SN/OE;
OX –10.7914/SN/OX; **RF** –10.7914/SN/RF; **SJ** – 10.7914/SN/SJ;
SL –10.7914/SN/SL; **Y5** –10.12686/SED/NETWORKS/Y5;
Z3 –10.12686/alparray/z3_2015.

Ekström, G., Nettles, M., and Dziewonski, A. M. (2012): The global CMT project 2004–2010: Centroid-moment tensors for 13,017 earthquakes, *Phys. Earth Planet. Inter.*, **200–201**, 1–9, https://doi.org/10.1016/j.pepi.2012.04.002.

Faivre, S., Lončar, N., Tomljenović, B., Sečanj, M., Herak, M., and Barešić, J. (2024): Impact of co-seismic uplifting on relative sea level change in the Southern Adriatic during the past 4.500 years

– New evidence from Dubrovnik epicentral area based on analysis of algal rims and tidal notches, *Geomorphology*, **460**, 109262, https://doi.org/10.1016/j.geomorph.2024.109262.

Ferrari, G. (2016): The contribution of the Sismos project to the preservation and dissemination of the material heritage of instrumental seismology, *Abstract, 35th General Assembly of the European Seismological Commission*, Trieste, 4–10 September 2016.

van Gelder, I. E., Matenco, L., Willingshofer, E., Tomljenović, B., Andriessen, P. A. M., Ducea, M. N., Beniest, A., and Gruić, A, (2015): The tectonic evolution of a critical segment of the Dinarides-Alps connection: Kinematic and geochronological inferences from the Medvednica Mountains, NE Croatia, *Tectonics*, **34**, 1952–1978, https://doi.org/10.1002/2015TC003937.

Govorčin, M., Herak, M., Matoš, B., Pribičević, B., and Vlahović, I. (2020): Constraints on complex faulting during the 1996 Ston–Slano (Croatia) earthquake inferred from the DInSAR, seismological, and geological observations, *Remote Sens.*, **12**, 1157, https://doi.org/10.3390/rs12071157.

Grenerczy, G., Sella, G., Stein, S., and Kenyeres, A. (2005): Tectonic implications of the GPS velocity field in the northern Adriatic region, *Geophys. Res. Lett.* **32**, L16311. https://doi.org/10.1029/2005GL022947.

Hardebeck, J. L., and Michael, A. J. (2006): Damped regional-scale stress inversions: Methodology and examples for southern California and the Coalinga aftershock sequence, *J. Geophys. Res.*, **111**, B11310, https://doi.org/10.1029/2005JB004144.

Heidbach, O., Barth, A., Müller, B., Reinecker, J., Stephansson, O., Tingay, M., Zang, A. (2016a): WSM quality ranking scheme, database description and analysis guidelines for stress indicator. *World Stress Map Technical Report 16-01*, GFZ German Research Centre for Geosciences. https://doi.org/10.2312/wsm.2016.001.

Heidbach, O., Rajabi, M. Reiter, K., Ziegler, M., and WSM Team (2016b): *World Stress Map Database Release 2016.* V. 1.1. GFZ Data Services, https://doi.org/10.5880/WSM.2016.001.

Heidbach, O., Rajabi, M., Cui, X., Fuchs, K., Müller, B., Reinecker, J., Reiter, K., Tingay, M., Wenzel, F., Xie, F., Ziegler, M. O., Zoback, M.-L., and Zoback, M. D. (2018): The World Stress Map database release 2016: Crustal stress pattern across scales, *Tectonophysics*, **744**, 484-498, https://doi.org/10.1016/j.tecto.2018.07.007

Herak, D. and Herak, M. (2010): The Kupa Valley (Croatia) earthquake of 8 October 1909 – 100 years later, *Seismol. Res. Lett.*, **81,** 30–36, https://doi.org/10.1785/gssrl.81.1.30.

Herak, D., Herak, M., Sović, I., and Markušić, S. (1991) Seismicity of Croatia in 1989 and the Kamešnica Mt. earthquake, *Geofizika*, **8**, 83–99.

Herak, M. (2008): ModelHVSR – A Matlab Tool to Model Horizontal-to-Vertical Spectral Ratio of Ambient Noise, *Comput. Geosci.*, **34**, 1514–1526.

Herak, M. and Herak, D. (2023): Properties of the Petrinja (Croatia) earthquake sequence of 2020–2021 – results of seismological research for the first six months of activity, *Tectonophysics*, **858**, 229885, https://doi.org/10.1016/j.tecto.2023.229885.

Herak, M. and Jukić, M. (1993): Fault-plane solution for the earthquake of 25 November 1986 near Knin, Croatia, *Geofizika*, **10**, 61–68.

Herak, M., Herak, D., and Markušić, S. (1995): Fault-plane solutions for earthquakes (1956–1995) in Croatia and neighbouring regions, *Geofizika*, **12**, 43–56.

Herak, M., Herak, D., and Markušić, S. (1996): Revision of the earthquake catalogue and seismicity of Croatia, 1908–1992, *Terra Nova*, **8**, 86–94.

Herak, M., Herak, D., and Orlić, N. (2021): Properties of the Zagreb 22 March 2020 earthquake sequence – analyses of the full year of aftershock recording, *Geofizika*, **38**, 93–116, https://doi.org/10.15233/gfz.2021.38.6.

Herak, D., Herak, M., Prelogović, E., Markušić, S., Markulin, Ž. (2005): Jabuka island (Central Adriatic Sea) earthquakes of 2003, *Tectonophysics*, **397**, 167–180.

INGV (2024): http://seismogramrequest.rm.ingv.it/, Istituto Nazionale di Geofisica e Volcanologia, Rome, Italy (last visited 2 September 2024).

International Seismological Centre (1992–2024): *On-line Bulletin*, https://doi.org/10.31905/D808B830.

Ivančić, I., Herak, D., Herak, M., Allegretti, I., Fiket, T., Kuk, K., Markušić, S., Prevolnik, S., Sović, I., Dasović, I., and Stipčević, J. (2018): Seismicity of Croatia in the period 2006–2015, *Geofizika*, **35**, 69–98, https://doi.org/10.15233/gfz.2018.35.2.

Ivančić, I., Herak, D., Markušić, S., Sović, I., and Herak, M. (2001): Seismicity of Croatia in the period 1997–2001, *Geofizika*, **18–19**, 17–29.

Ivančić, I., Herak, D., Markušić, S., Sović, I., and Herak, M. (2006): Seismicity of Croatia in the period 2002– 2005, *Geofizika*, **23**, 1–17.

Kagan, Y. Y. (1991): 3-D rotation of double-couple earthquake sources, *Geophys J. Int.*, **106**, 709–716, https://doi.org/10.1111/j.1365-246x.1991.tb06343.x.

Kawasumi, H. (1934): Study on the Propagation of Seismic Waves (The second paper), Amplitude of Seismic Waves with the Structure of the Earth's Crust and Mechanisms of their Origin, *Bull. Earthq. Res. Inst.*, Tokyo Imperial University, **12**, 660–705.

Lentas, K., Di Giacomo, D., Harris, J., and Storchak, D. A. (2019): The ISC Bulletin as a comprehensive source of earthquake source mechanisms, *Earth Syst. Sci. Data*, **11**, 565–578, https://doi.org/10.5194/essd-11-565-2019.

Lund B. and Townend, J. (2007): Calculating horizontal stress orientations with full or partial knowledge of the tectonic stress tensor, *Geophys J. Int.*, **170**, 1328-1335, https://doi.org/10.1111/j.1365-246X.2007.03468.x.

Markušić, S., Herak, D., Ivančić, I., Sović, I., Herak, M., and Prelogović, E. (1998): Seismicity of Croatia in the period 1993–1996 and the Ston-Slano earthquake of 1996, *Geofizika*, **15**, 83–101.

Markušić, S., Herak, D., Sović I., and Herak, M. (1993): Seismicity of Croatia in the period 1990–1992, *Geofizika*, **10**, 19–34.

Martínez-Garzón, P., Ben-Zion, Y., Abolfathian, N., Kwiatek, G., and Bohnhoff. M. (2016): A refined methodology for stress inversions of earthquake focal mechanisms, *J. Geophys. Res., Solid Earth*, **121**, 8666–8687, https://doi.org/10.1002/2016JB013493.

Martínez-Garzón, P., Kwiatek, G., Ickrath, M. and M. Bohnhoff (2014): MSATSI: A MATLAB package for stress inversion combining solid classic methodology, a new simplified user-handling and a visualization tool, *Seismol. Res. Lett.*, **85**, https://doi.org/10.1785/0220130189.

Matoš, B., Tomljenović, and Trenc, B. (2014): Identification of tectonically active areas using DEM: a quantitative morphometric analysis of Mt. Medvednica, NW Croatia, *Geol. Q.*, **58**, 51–70, https://doi.org/http://dx.doi.org/10.7306/gq.1130.

Mayeda, K., Koyanagi, S., Hoshiba, M., Aki, K., and Zeng, Y., (1992): A comparative study of scattering, intrinsic, and coda Q^{-1} for Hawaii, Long Valley, and central California between 1.5 and 15.0 Hz, *J. Geophys. Res.*, **97**, 6643–6659, https://doi.org/10.1029/91JB03094.

McKenzie, D. (1972): Active Tectonics of the Mediterranean Region, *Geophys. J. Roy. Astron. Soc.,* **30**, 109–185, https://doi.org/10.1111/j.1365-246X.1972.tb02351.x.

Mohorovičić, A. (1910a): Potres od 8. X 1909, *Godišnje izvješće Zagrebačkog meteorološkog opservatorija za godinu 1909*, **9** (4), 1–56.

Mohorovičić, A. (1910b): Das Beben vom 8. X. 1909, *Jahrbuch des meteorologischen Observatoriums in Zagreb (Agram) für das Jahr 1909*, **9** (4), 63 pps.

Mohorovičić, A. (1910c): Earthquake of 8 October 1909, Reprinted in *Geofizika*, **9** (1992), 3–55.

Moulin, A., Benedetti, L., Gosar, A., Jamšek Rupnik, P., Rizza, M., Bourlès, D., Ritz, J.-F. (2014): Determining the present-day kinematics of the Idrija fault (Slovenia) from airborne LiDAR topography, *Tectonophysics*, **628** 188–205, https://dx.doi.org/10.1016/j.tecto.2014.04.043.

Moulin, A., Benedetti, L., Rizza, M., Jamšek Rupnik, P., Gosar, A., Bourles, D., Keddadouche, K., Aumaître, G., Arnold, M., Guillou, V., and Ritz, J. F. (2016): The Dinaric fault system: Large-scale structure, rates of slip, and Plio-Pleistocene evolution of the transpressive northeastern boundary of the Adria microplate, *Tectonics*, **35**, 2258–2292, https://doi.org/10.1002/2016TC004188.

Nakano, H. (1923). Notes on the nature of the forces which give rise to the earthquake motions, *Central Meteorological Observatory of Japan*, *Seismological Bulletin*, **1**, 92–130.

Nocquet, J.-M. and E. Calais (2004): Geodetic Measurements of Crustal Deformation in the Western Mediterranean and Europe, *Pure Appl. Geophys.*, **161**, 661–681, https://doi.org/10.1007/s00024-003-2468-z.

Palenik, D., Matičec, D., Fuček, L., Matoš, B., Herak, M. & Vlahović, I. (2019) Geological and structural setting of the Vinodol valley (NW Adriatic, Croatia): insights into tectonic evolution based on structural investigations, *Geol. Croat.*, **72** (3), 179–193, https://doi.org/10.4154/gc.2019.13.

Porkoláb, K., Békési, E., Győri, E., Broerse, T., Czecze, B., Kenyeres, A., Tari, G., and Wéber, Z. (2024): Present-day stress field, strain rate field and seismicity of the Pannonian region: overview and integrated analysis, *In:* Tari, G. C., Kitchka, A., Krézsek, C., Lučić, D., Markič, M., Radivojević, D., Sachsenhofer, R. F., Šujan, M. (Eds.) (2024): *The Miocene Extensional Pannonian Superbasin, Volume 1: Regional Geology*, Geological Society, London, Special publications, **554**, https://doi.org/10.1144/SP554-2023-219.

Rabinowitz, N. and Hofstetter, A. (1992): A rapid algorithm for estimating fault plane solution using polarity-amplitude data: application of a non-linear programming approach, *Phys. Earth Planet. Inter.*, **73**, 239–254, https://doi.org/10.1016/0031-9201(92)90094-C.

Ritsema, A. R. (1967): Mechanisms of European Earthquakes, *Tectonophysics*, **4**, 247–259, https://doi.org/10.1016/0040-1951(67)90034-0.

Roselli, P., Marzocchi, W., Mariucci, M. T., and Montone. P. (2018): Earthquake focal mechanism forecasting in Italy for PSHA purposes, *Geophys J. Int.*, **212**, 491–508, https://doi.org/10.1093/gji/ggx383.

Saraò, A., Sugan, M., Bressan, G., Renner, G., and Restivo, A. (2021): A focal mechanism catalogue of earthquakes that occurred in the southeastern Alps and surrounding areas from 1928–2019, *Earth Syst. Sci. Data*, **13**, 2245–2258, https://doi.org/10.5194/essd-13-2245-2021.

Schmid, S. M., Bernoulli, D., Fügenschuh, B., Matenco, L., Schefer, S., Schuster, R., Tischler, M., and Ustaszewski, K. (2008): The Alpine-Carpathian-Dinaridic orogenic system: correlation and evolution of tectonic units, *Swiss J. Geosci.*, **101**, 139–183.

Schmid, S. M., Fügenschuh, B., Kounov, A., Mațenco, L., Nievergelt, P., Oberhänsli, R., Pleuger, J., Schefer, S., Schuster, R., Tomljenović, B., Ustaszewski, K., and van Hinsbergen, D. (2020): Tectonic units of the Alpine collision zone between Eastern Alps and western Turkey, *Gondwana Res.,* **78**, 308–374, https://doi.org/10.1016/j.gr.2019.07.005.

Stauder, S. J. W. (1962): The Focal Mechanism of Earthquakes, *Adv. Geophys.*, **9**, 1–76, https://doi.org/10.1016/S0065-2687(08)60527-0.

Stipčević, J., Tkalčić, H., Herak, M., Markušić, S., and Herak, D. (2011): Crustal and uppermost mantle structure beneath the External Dinarides, Croatia, determined from teleseismic receiver functions, *Geophys J. Int.*, **185** (3), 1103–1119. https://doi.org/10.1111/j.1365-26X.2011.05004.x.

Tomljenović, B. and L. Csontos (2001): Neogene-Quaternary structures in the border zone between Alps, Dinarides and Pannonian Basin (Hrvatsko zagorje and Karlovac Basins, Croatia), *Int. J. Earth Sci. (Geologische Rundschau),* **90**, 560–578, https://doi.org/10.1007/s005310000176.

Turhan, F., Acarel, D., Plicka, V., Bohnhoff, M., Polat, R. and Zahradník, J. (2023): Coseismic Faulting Complexity of the 2019 Mw 5.7 Silivri Earthquake in the Central Marmara Seismic Gap, Offshore Istanbul, *Seismol. Res. Lett.*, **94**, 75–86. https://doi.org/10.1785/0220220111.

Ustaszewski, K., Herak, M., Tomljenović, B., Herak, D., and Matej, S. (2014): Neotectonics of the Dinarides–Pannonian Basin transition and possible earthquake sources in the Banja Luka epicentral area. *J. Geodyn.*, **82**, 52–68, https://doi.org/10.1016/j.jog.2014.04.006.

Weber, J., Vrabec, M., Pavlovčič-Prešeren, P., Dixon, T., Jiang, Y., and Stopar, B. (2010): GPSderived motion of the Adriatic microplate from Istria Peninsula and Po Plain sites, and geodynamic implications, *Tectonophysics*, **483**, 214–222. https://doi.org/10.1016/j.tecto.2009.09.001.

Živčić, M. and Allegretti, I. (1983): Niz potresa u Kvarnerskom zaljevu u svibnju–lipnju 1979. godina, *Acta Seismol. Iugosl.*, **9**, 9–25 (in Croatian with English abstract).

Živčić, M., Mišković, D., Allegretti, I. (1980): Potresi 25. VII 1979. u Imotskom polju, *Acta Seismol. Iugosl.*, **6**, 29–37 (in Croatian with English abstract).

SAŽETAK

Hrvatski katalog i pripadna baza podataka žarišnih mehanizama potresa, karakteristični mehanizmi i svojstva polja napetosti u Dinaridima i susjednim područjima

Marijan Herak

U ovom je radu prikazan CroFMS katalog i pripadna baza podataka žarišnih mehanizama potresa. Temelji se na desetljećima prikupljanim podacima o polaritetu prvih pomaka P-valova potresa koji su se dogodili kako u Hrvatskoj, tako i u susjednim regijama čija bi seizmičnost mogla utjecati na potresnu opasnost u Hrvatskoj. Trenutna verzija kataloga sadrži žarišne mehanizme koji su sustavno izračunati koristeći iste programe, modele brzina, težinske faktore podataka, kao i pravila za određivanja pouzdanosti rješenja. Katalog sadrži mehanizme i druge prateće podatke za 410 potresa koji su se dogodili do 30. lipnja 2024. U članku su prikazane razdiobe vremena i izvora očitanih polariteta, magnituda potresa, epicentralnih udaljenosti postaja, ocjena kvalitete, korištenih faza, i dr. Također je pokazano da su rješenja temeljena na polaritetima prvih pomaka iz CroFMS kataloga i ona neovisno dobivena inverzijom tenzora momenta koju su provele razne međunarodne agencije, uglavnom konzistentne.

Usporedba promatranih žarišnih mehanizama s najnovijim europskim modelom rasjednih izvora potresa (EFSM20) otkrila je nekoliko neslaganja, osobito u epicentralnim područjima Zagreba i Petrinje, širem riječkom području, srednjejadranskim otocima te u zoni čela navlaka Istočna Bosna–Durmitor i Drina–Ivanjica u Bosni i Hercegovini.

Prostorno usrednjavanje žarišnih mehanizama za cijelo istraživano područje rezultiralo je katalozima i odgovarajućim kartama karakterističnih žarišnih mehanizama. One bi mogle biti korisne u procjeni seizmičke opasnosti u područjima u kojima aktivni rasjedi još nisu identificirani ili karakterizirani.

Formalna inverzija napetosti iz izračunatih žarišnih mehanizama rezultirala je kartom orijentacije maksimalne horizontalne napetosti (S_{Hmax}) u istraživanom području na kojoj su vidljive lokalne lateralne varijacije koje nisu bile identificirane ranijim istraživanjima. Primjer je promjena orijentacije S_{Hmax} za približno 35° u smjeru suprotnom od kazaljke na satu između čela Predkrške navlake i zone čela navlaka Drina–Ivanjica i Istočna Bosna–Durmitor.

Ključne riječi: žarišni mehanizmi potresa, karakteristični žarišni mehanizmi, polje napetosti, glavne osi napetosti

Corresponding author's address: Professor emeritus Marijan Herak, Department of Geophysics, Faculty of Science, University of Zagreb, Horvatovac 95, 10000 Zagreb, Croatia; e-mail: mherak@gfz.hr

Appendix A

A1. First-motion polarities inversion method

The best fitting double-couple parameters are sought by exhaustive grid-search (with the resolution of 2°) for the triplet [φ_0 – strike, δ_0 – dip, λ_0 – rake] that minimizes the misfit function D defined for N observations as:

$$D(\varphi,\delta,\lambda) = \frac{\sum_{i=1}^{N} w_i \left[r_i(\varphi,\delta,\lambda) - p_i \right]^2}{\sum_{i=1}^{N} w_i} \left[\frac{100}{g(\varphi,\delta,\lambda)} \right]^k \qquad (A1)$$

where r is the theoretical radiation pattern amplitude, p is the observed normalized amplitude of the P-wave first onset, and w is the corresponding weight. The individual weights w,

$$w = w_{ie} w_r w_{sb},$$

depend on whether the onset is clear (i) or emergent (e) (here $w_{ie}(i) = 1.00$, $w_{ie}(e) = 0.50$, otherwise $w_{ie} = 0.75$), how close is the station to the nodal line (because there is large probability for wrong reading if it is close to the nodal line; here we used $0.5 < w_r < 1.0$), and whether it is a bulletin datum or read from the seismogram by the analyst (here $w_{sb} = 1.00$ for data read from the seismogram, and $w_{sb} = 0.50$ for the bulletin data). g is the percentage of correct polarities for the choice (φ, δ, λ) (ranging from 50% to 100%). The last factor in (A1) gives preference among similar solutions to the ones with larger number of correct polarities. Exponent k determines the relative role that $g(\varphi, \delta, \lambda)$ has – $k = 0.0$ gives all weight to the first factor in (A1), while large k shifts the influence heavily towards the percentage of correct polarities. For most of the cases with data read from the seismograms k was kept in the range $1.0 < k < 4.0$, whereas for the bulletin-dominated datasets k was increased to larger values.

The observable p may be simply ±1 (polarity), but it may also be discretized into any number of classes between 0.0 and ±1.0 indicating the amplitude of the first swing corresponding to the analyst's qualitative estimate of r. For instance, ±0.1, ±0.3, ±0.5, ±0.7, ±0.9, may signify first amplitudes that are described as "very small" (probably close to the nodal line where $r = 0.0$), "small", "average; about as expected for that phase", "large", and "very large" (probably close to the centre of the quadrant, $r = \pm 1.0$), respectively. r in (A1) is discretized in the same way as p. A very similar approach was suggested by Rabinowitz and Hofstetter (1992), who used a three-class scheme (small, normal and large first amplitude) in their flexible tolerance method. The applicability of such a scheme depends on several reasonable first-order assumptions (for discussion see Rabinowitz and Hofstatter, 1992). Obviously, estimates of p are subjective, but – in my experience – a skilled analyst generally makes reasonable assessments thus retrieving more information from seismograms than by a simple binary choice of '+1' or '–1'.

Inclusion of the amplitude proxy for the radiation pattern may help in discriminating between competing solutions in case when polarities alone do not provide enough constraint. This is often the case when networks are sparse, the stations are unevenly distributed, and/or most first arrivals are *Pn*. Typical examples are the earthquakes in the Adriatic Sea, with very few close-by stations, and a poor coverage of the northwesterly and southeasterly directions, or the events in the Dinarides which typically occur close to the coast on reverse faults whose dip is similar to the take-off angle of *Pn*, thus mapping many of such observations along the nodal lines.

Once D has been determined for all combinations of (φ, δ, λ), it is possible to extract the set of solutions that are within the desired confidence limits, c_L. This is done by normalizing all misfits functions by the smallest one, $f_i = D_i/D_0$, and by computing the F-function cumulative distribution $F_i = \mathrm{CDF}(f_i, N–m, N–m)$, where D_i and D_0 are the misfit functions for the i-th combination of (φ_i, δ_i, λ_i) and for the best fitting one (φ_0, δ_0, λ_0), respectively, N is the number of observations and $m = 3$ is the number of varied model parameters (*e.g.* Mayeda *et al.*, 1992; Bianco *et al.* 2002; see also Herak, 2008; Stipčević *et al.*, 2011). I chose $c_L = 0.75$, and retained for statistical analyses all solutions with $F_i < c_L$. Based on the percentage of correct polarities g_0, and the maximum Kagan angle ($\alpha_{\max}$; Kagan, 1991) between the best solution and all other solutions within the confidence interval, criteria for the quality Q of a solution (1 – unacceptable, ... 5 – the best) are defined as:

$Q = 1$: $\alpha_{\max} \geq 45°$ or $g_0 < 75\%$ [Unacceptable]
$Q = 2$: $\alpha_{\max} < 45°$ and $g_0 \geq 75\%$ [Marginally acceptable]
$Q = 3$: $\alpha_{\max} < 28°$ and $g_0 \geq 80\%$ and $g_0 < 85\%$ [Good]
$Q = 4$: $\alpha_{\max} < 20°$ and $\alpha_{\max} \geq 15°$ and $g_0 \geq 85\%$ [Very good]
$Q = 5$: $\alpha_{\max} < 15°$ and $g_0 \geq 85\%$ [Excellent],

where the strictest fullfiled conditions apply.

The Kagan angle (α) between two focal mechanism solutions is defined as the least solid angle needed to rotate one solution into the other. It can attain values between 0° and 120°. It is generally accepted that α with a value between 20° and 30° indicates very similar solutions (*e.g.* Lentas et al., 2019; Saraò et al., 2021).

A2. Velocity models

Figure A1 shows three general P-wave velocity models used to compute the takeoff angles of the first P-phases (P_1) using the *TauP* toolkit (Crotwell et al., 1999), which are applied when the source is within the External Dinarides (green), Adriatic (blue) or elsewhere (red). They differ the most in the thickness of the crust. In studies of smaller areas or studies of aftershock sequences, if local models were available based on earthquake locations, those were used in

focal mechanism inversions too (*e.g.* Govorčin et al., 2020; Herak etal.,2021; Herak and Herak, 2023; Dasović et al., 2024).

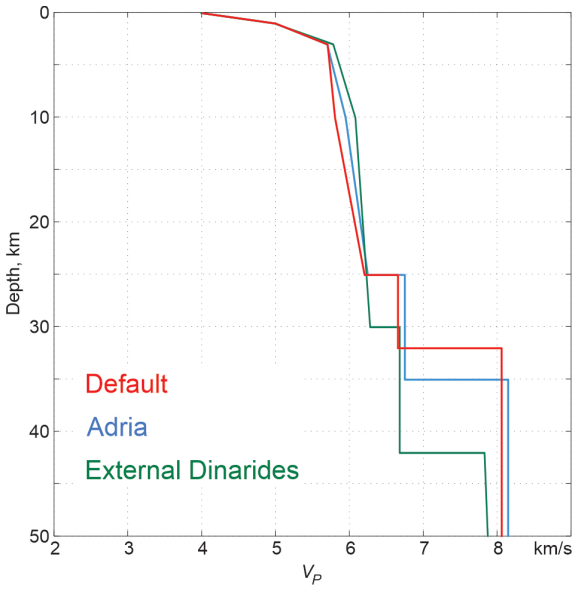

Figure A1. The three P-wave velocity models used to estimate the takeoff angle from the focus, when the earthquake occurred in the External Dinarides (green), the Adriatic (blue) or elsewhere (green).

Appendix B – Additional figures

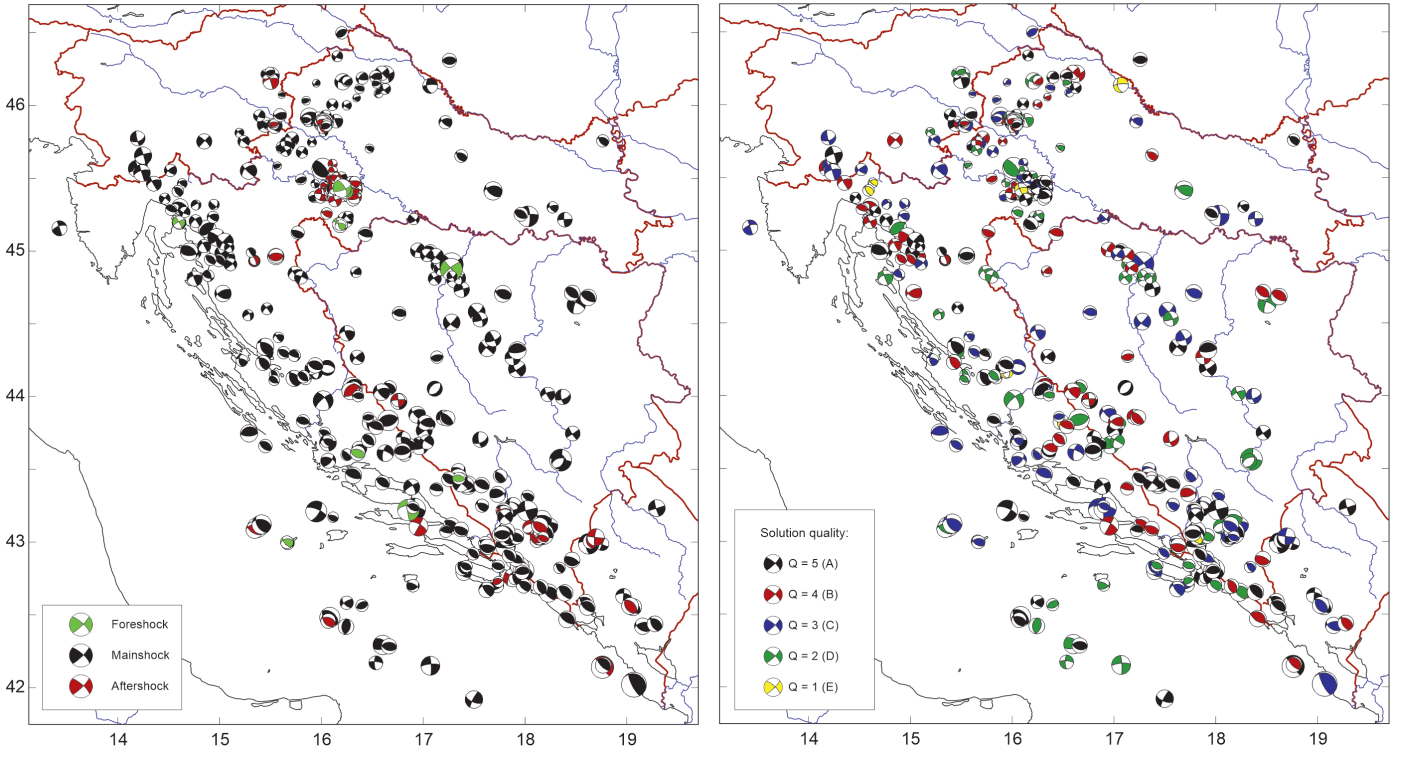

Figure B1. FMS from CroFMS catalogue (focal depths less than 35 km) classified: *Left*: as foreshocks, mainshocks, and aftershocks; *Right:* by the solution quality.

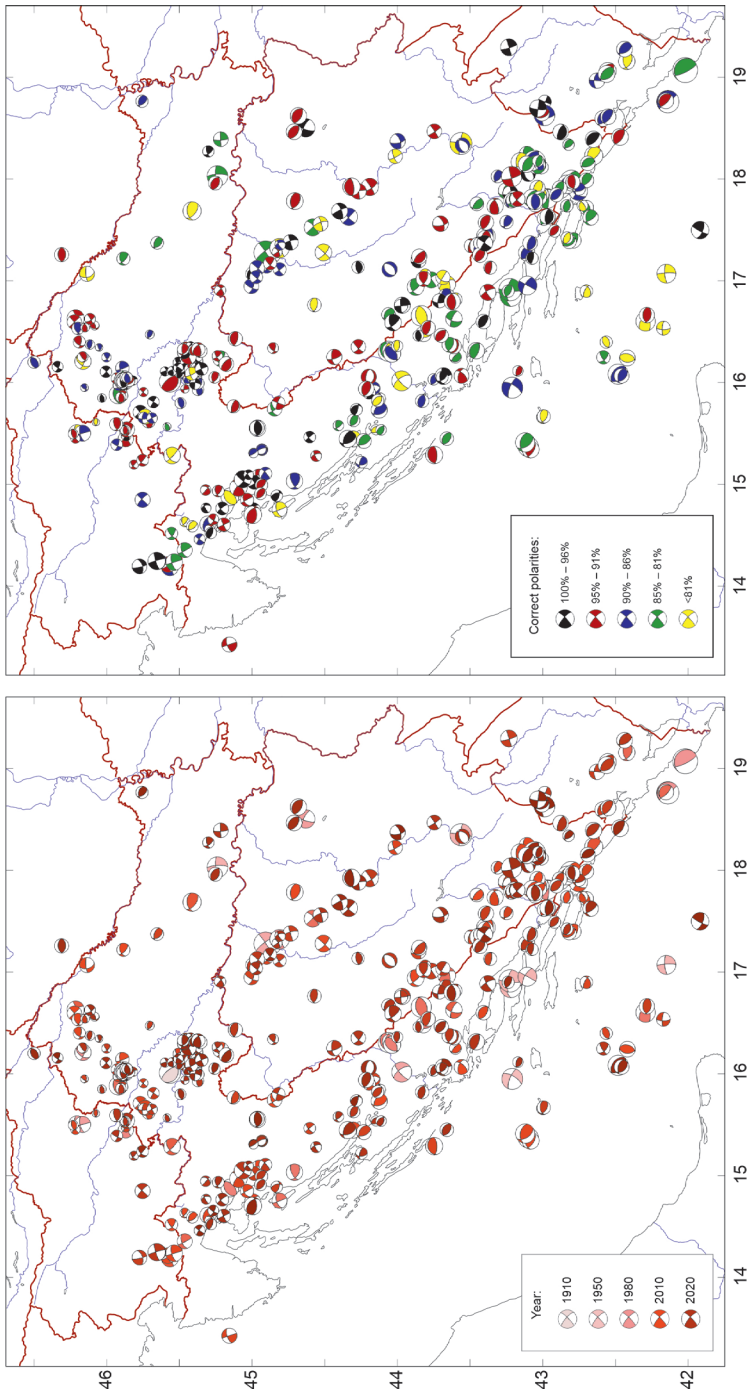

Figure B2. FMS from CroFMS catalogue (focal depths less than 35 km) classified by: *Left*: Year of occurrence; *Right*: The percentage of correct first-motion polarities.

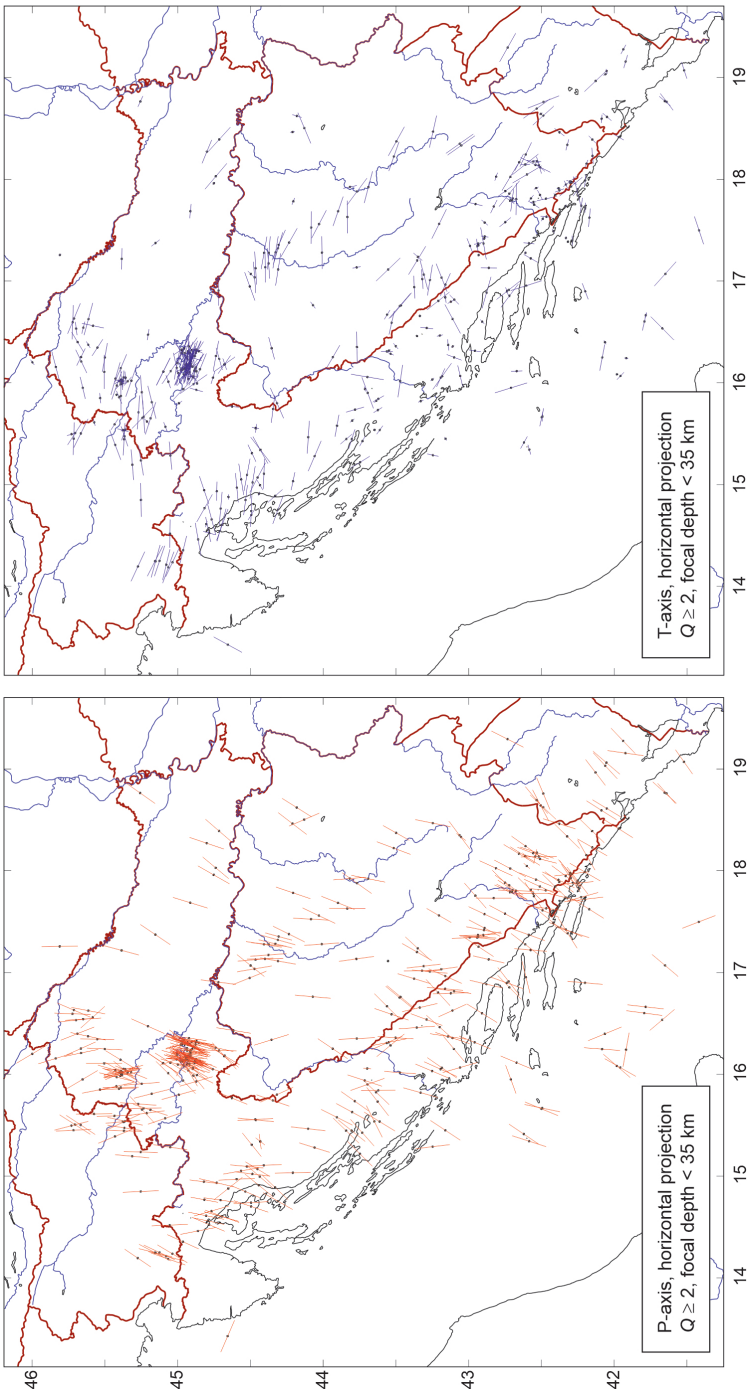

Figure B3. Horizontal projection of: *Left*: P-axes, and *Right*: T-axes, for FMS with quality $Q \geq 2$ and earthquake foci above 35 km.

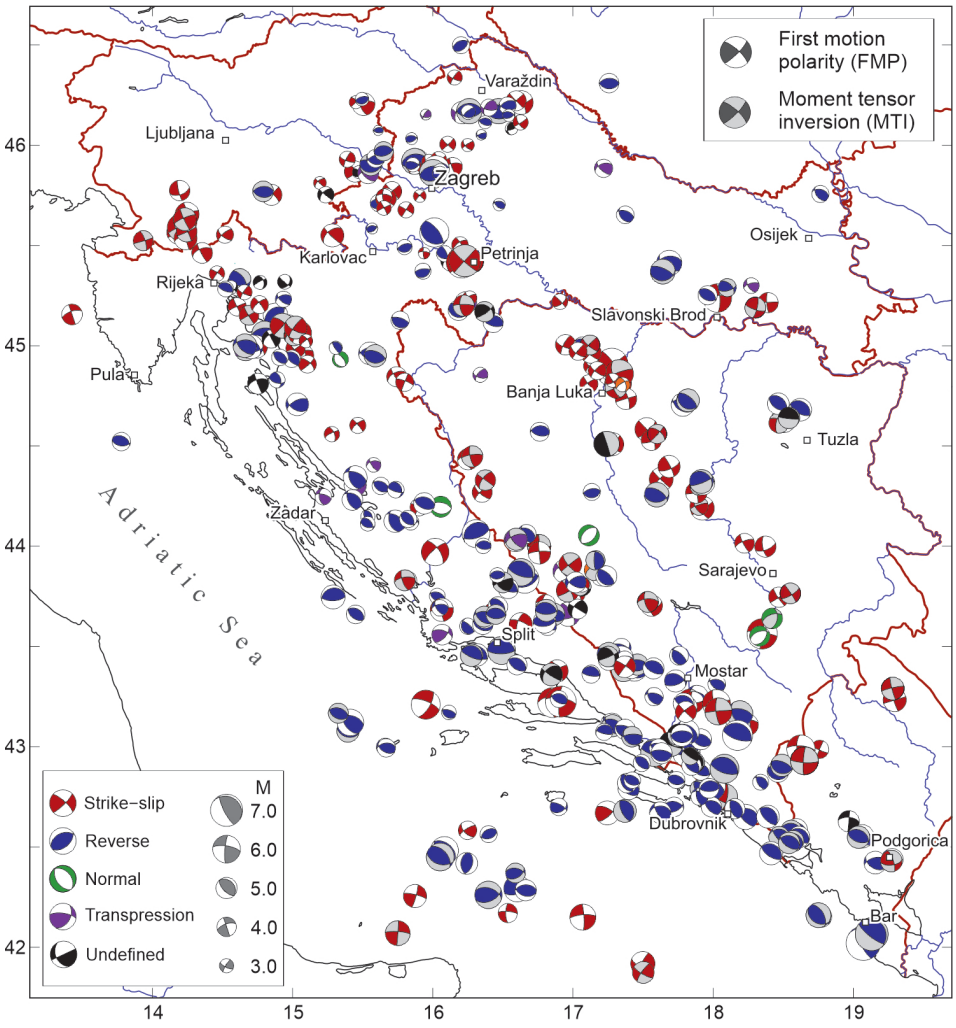

Figure B4. FMP focal mechanisms from the CroFMS catalogue (white dilatation quadrants), and available BDC solutions from the moment-tensor inversion (grey dilatation quadrants; see caption to Fig. 13 for sources). Aftershocks are not considered.

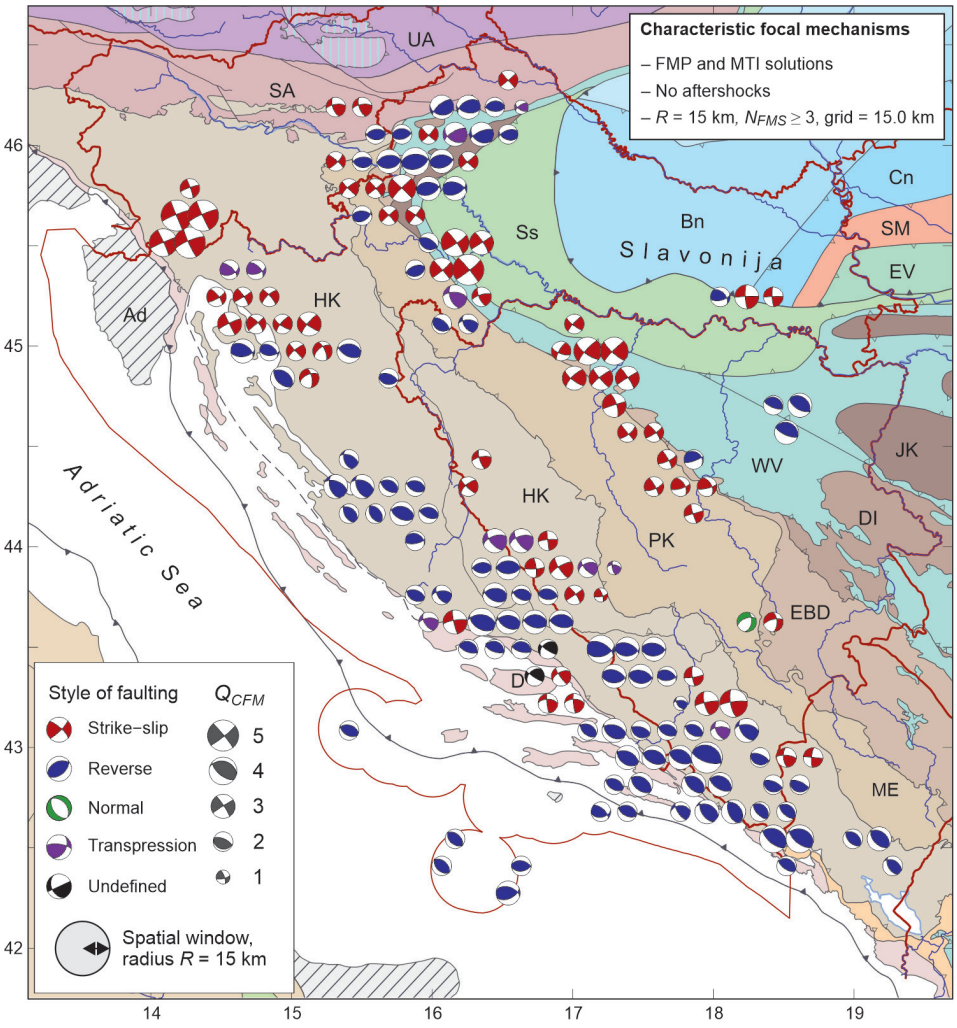

Figure B5. Characteristic focal mechanisms (CFM) computed by weighted averaging of the FMP focal mechanisms and MTI solutions on a grid 15.0 km × 15.0 km, within the spatial window with radius of $R = 15$ km. Aftershocks were not considered. Only solutions based on at least three events in the window are shown. The size of the beachballs scales with the quality Q_{CFM}. The basemap of tectonic units is simplified after Shmid et al. (2020, see caption of Fig. 7 for detailed explanation).

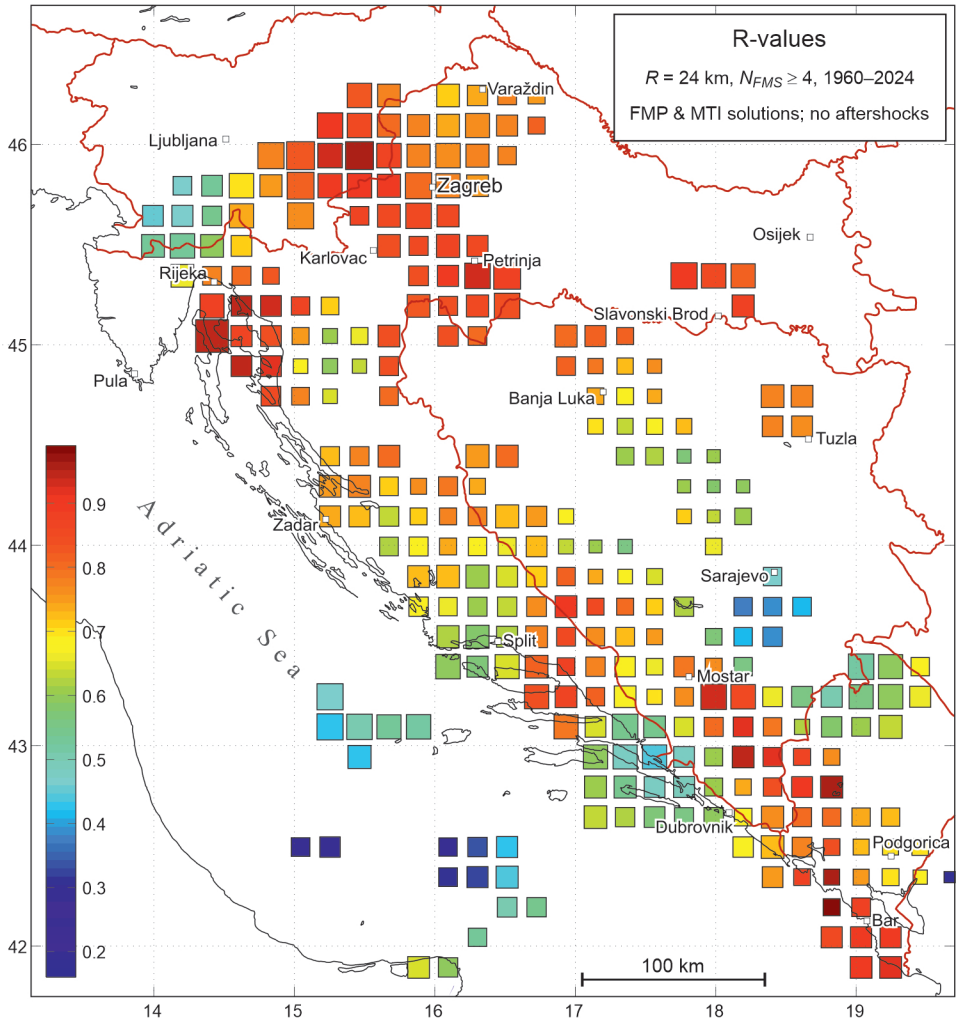

Figure B6. Spatial variation of the relative stress magnitude [R-value = $(\sigma_1 - \sigma_2) / (\sigma_1 - \sigma_3)$].

Electronic supplement

Three FMS catalogues in the form of Excel-files are available for free download:

1. The CroFMS catalogue – file: **CroFMS_2024.xlsx**
2. The catalogue of characteristic focal mechanisms based on first-motion polarity solutions only – file: **Characteristic_FMP_2024.xlsx**
3. The catalogue of characteristic focal mechanisms based on the first-motion polarity solutions and the best double-couple solutions by the moment inversion – file: **Characteristic_FMP_MTI_2024.xlsx**

The first row is the header: **N** – *Serial number of FMS*; **Year**; **Month**; **Day**; **Hour**; **Minute**; **Second**; **Lat.** – *latitude °N*; **Lon.** – *longitude °E*: **Depth** – *in km*; **M** – *magnitude* M_L; **NP1str** – *strike of nodal plane 1*; **NP1dip** – *dip of nodal plane 1*; **NP1rake** – *rake of nodal plane 1*; **NP2str** – *strike of nodal plane 2*; **NP2dip** – *dip of nodal plane 2*; **NP2rake** – *rake of nodal plane 2*; **Pst** – *strike of the P-axes*; **Pdip** – *dip (plunge) of the P-axes*; **Tst** – *strike of the T-axes*; **Tdip** – *dip (plunge) of the T-axes*; **Qual** – *Quality of solution (1–5).*

None of the two nodal planes is the preferred one. The catalogues are up to date until 30 June 2024.